HHS Public Access

Author manuscript

Cell Rep. Author manuscript; available in PMC 2024 April 10.

Published in final edited form as:

Cell Rep. 2024 March 26; 43(3): 113876. doi:10.1016/j.celrep.2024.113876.

Ly6C$^+$ monocytes in the skin promote systemic alphavirus dissemination

Autumn C. Holmes[1], **Cormac J. Lucas**[2], **Morgan E. Brisse**[3], **Brian C. Ware**[2], **Heather D. Hickman**[3], **Thomas E. Morrison**[2], **Michael S. Diamond**[1,4,5,6,7,8,*]

[1]Department of Medicine, Washington University School of Medicine, St. Louis, MO, USA

[2]Department of Immunology and Microbiology, University of Colorado School of Medicine, Aurora, CO, USA

[3]Viral Immunity and Pathogenesis Unit, Laboratory of Clinical Microbiology and Immunology, National Institutes of Allergy and Infectious Diseases, NIH, Bethesda, MD, USA

[4]Department of Molecular Microbiology, Washington University School of Medicine, St. Louis, MO, USA

[5]Department of Pathology & Immunology, Washington University School of Medicine, St. Louis, MO, USA

[6]Andrew M. and Jane M. Bursky the Center for Human Immunology and Immunotherapy Programs, Washington University School of Medicine, St. Louis, MO, USA

[7]Center for Vaccines and Immunity to Microbial Pathogens, Washington University School of Medicine, St. Louis, MO, USA

[8]Lead contact

SUMMARY

Alphaviruses are mosquito-transmitted pathogens that induce high levels of viremia, which facilitates dissemination and vector transmission. One prevailing paradigm is that, after skin inoculation, alphavirus-infected resident dendritic cells migrate to the draining lymph node (DLN), facilitating further rounds of infection and dissemination. Here, we assess the contribution of infiltrating myeloid cells to alphavirus spread. We observe two phases of virus transport to the DLN, one that occurs starting at 1 h post infection and precedes viral replication, and a second that requires replication in the skin, enabling transit to the bloodstream. Depletion of Ly6C$^+$ monocytes reduces local chikungunya (CHIKV) or Ross River virus (RRV) infection in the skin,

*Correspondence: mdiamond@wustl.edu.

AUTHOR CONTRIBUTIONS

A.C.H. performed cell depletions, mouse infection, tissue harvesting, RT-qPCR, flow cytometry, and plaque assays. C.J.L. performed lymphatic transport assays and imaging of FITC-dextran accumulation in DLNs. M.E.B. performed DLN staining, imaging, and quantification experiments. B.C.W. generated the CHIKV-Venus cDNA clone. T.E.M., H.D.H., and M.S.D. supervised studies and provided resources for the experiments. A.C.H. and M.S.D. designed studies and wrote the initial draft. All other authors provided editorial comments.

SUPPLEMENTAL INFORMATION

Supplemental information can be found online at https://doi.org/10.1016/j.celrep.2024.113876.

diminishes the second phase of virus transport to the DLN, and delays spread to distal sites. Our data suggest that infiltrating monocytes facilitate alphavirus infection at the initial infection site, which promotes more rapid spread into circulation.

Graphical Abstract

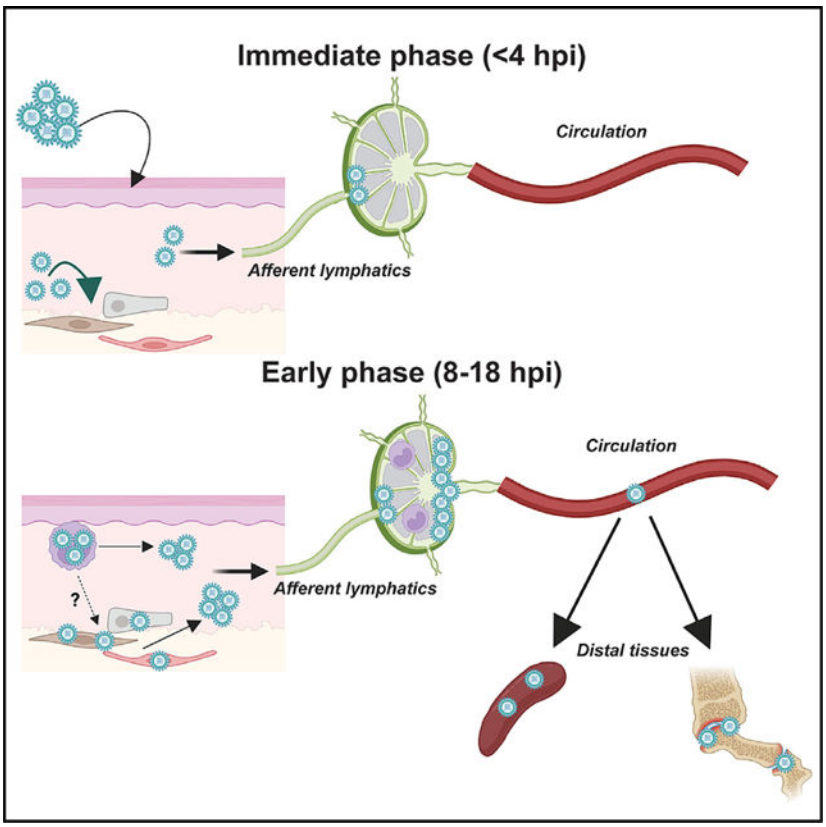

In brief

Holmes et al. demonstrate that infiltrating Ly6C^{hi} monocytes in the skin facilitate dissemination of CHIKV through the lymphatics into circulation. Monocytes in the skin become infected and boost the amount of CHIKV produced by nearby stromal cells, resulting in enhanced virus transit to the draining lymph node and systemic spread.

INTRODUCTION

Alphaviruses are mosquito-transmitted RNA viruses that can cause systemic, cutaneous, musculoskeletal, or central nervous system disease. Alphaviruses are maintained in a sylvatic cycle in nature[1] with wild primates, rodents, and passerine birds acting as amplification hosts depending on the specific virus and complex. Alphaviruses in the Semliki Forest (SF) complex, including chikungunya (CHIKV), Ross River (RRV), Mayaro (MAYV), and o'nyong'nyong (ONNV) viruses, infect and cause injury to musculoskeletal cells. CHIKV has been responsible for large-scale global epidemics of acute arthritis, which can progress to chronic musculoskeletal disease in a subset of afflicted individuals.[2] CHIKV

and some other alphaviruses can establish urban epidemic transmission cycles, with human hosts amplifying virus to high levels in the blood,[3] enabling efficient transmission to vector mosquitoes during a blood meal.

Within a vertebrate host, alphaviruses can spread via lymphatic or hematogenous routes to disseminate from the primary inoculation site to distant target sites in visceral and other organs. After mosquito inoculation in the skin, alphaviruses are thought to replicate first in Langerhans cells (LCs)[3] and dermal fibroblasts,[4] traffic to the local draining lymph node (DLN) within migratory LCs,[5] productively replicate within the DLN, and then enter circulation via efferent flow of lymph into the thoracic duct. Alphavirus spread via the lymphatics is considered one of the earliest steps in the dissemination process prior to establishing viremia. However, recent work demonstrated that macrophage receptor with collagenous structure (MARCO), a scavenger receptor on lymphatic endothelial cells (LECs), filters virus and limits CHIKV and RRV transit into the circulation.[6,7] Early innate immune responses in the skin also may modulate dissemination of some alphaviruses, including SF virus (SFV)[8] and RRV[5]; neutrophil-driven inflammatory responses induced by mosquito saliva enhanced SFV spread in a manner dependent on the chemokine receptor CCR2.[8] Neutrophil and CX3CR1^{+} monocyte infiltration into the skin and DLN also has been observed after intradermal injection of RRV, although a direct role for leukocyte-mediated spread in RRV pathogenesis was not assessed.[5] Notwithstanding these data, infiltrating leukocytes into the skin also have antiviral roles in limiting viral dissemination; CCR2^{+} monocytes can restrict RRV infection through a mitochondrial antiviral signaling (MAVS) protein-dependent type I interferon (IFN) response.[9]

A key unanswered question in alphavirus pathogenesis is whether immigrant immune cells in the skin become productively infected and, if so, how this contributes to viral dissemination. While alphavirus infection of monocytes has been demonstrated *in vitro*[10,11] and in the bloodstream of mice, replication is limited by innate immune signals generated by the microbiome and translated by plasmacytoid dendritic cells (DCs).[12] We sought to define the role of infiltrating myeloid cells in alphavirus infection in the skin and dissemination soon after inoculation. Within 1 h of inoculation in the skin, CHIKV transited to the DLN, and this occurred independently of replication or infiltrating myeloid cells. However, depletion of Ly6C^{+} monocytes resulted in a decrease in subsequent accumulation of CHIKV and RRV in the DLN and dissemination to the blood, spleen, and musculoskeletal tissues distal to the site of initial infection, as well as reduced infection in non-hematopoietic cells in the skin. Related to this observation, productive CHIKV infection was observed within a fraction of Ly6C^{+} monocytes in the skin at 18 and 36 h post infection (hpi). The effects on virus accumulation in the DLN required active infection, as lymphatic transit of Aura (AURV) or Eilat (EILV)/CHIKV chimeric viruses, alphaviruses that do not replicate efficiently in murine cells, or soluble dextran, was unaffected by depletion of Ly6C^{+} myeloid cells. Our data support a model whereby, within hours of inoculation in the skin, non-cell-associated alphavirus transits to the DLN via lymphatics independently of infiltrating myeloid cells, and this virus is likely captured by MARCO on LECs. However, at later time points (i.e., after 8 hpi), infiltrating Ly6C^{+} myeloid cells that are infected in the skin promote local virus replication and enhance transport of virus to the DLN, which may

overcome the MARCO/LEC barrier, enabling dissemination to the bloodstream and spread to distal sites.

RESULTS

Depletion of myeloid cells impairs CHIKV dissemination

Myeloid cells have been shown to act as vehicles for the spread of many viruses within the host.[13] As an early myeloid cell response is elicited at the initial site of alphavirus inoculation,[5] we evaluated their possible contribution to virus infection and dissemination. We first performed a time course of infection in 4-week-old C57BL/6J mice after footpad inoculation of CHIKV to define the earliest time point that CHIKV (La Reunion-2006 [LR] strain) enters the circulation (Figures 1A and 1B). Viral RNA was not detected in the serum or spleen at 1 or 4 hpi. While a few animals had measurable viral RNA in the serum and spleen at 8 hpi, all animals had detectable viral RNA at 18 hpi. We thus chose the 18-hpi time point for further analysis of the effects of myeloid cells on virus dissemination. To test the impact of myeloid cells on CHIKV-LR dissemination, we treated mice with an anti-Ly6C/Ly6G monoclonal antibody (mAb) (anti-GR-1 mAb, clone RB6–8C5) that depletes monocytes, neutrophils, and some other granulocyte populations (Figure S1[14]) or an isotype control antibody We administered anti-GR-1 or control mAb 1 day prior to infection; inoculated mice with virus in the left rear footpad; and then collected serum, spleen, and ipsilateral and contralateral foot tissues at 18 hpi. Notably, depletion of Ly6C/Ly6G myeloid cells resulted in reduced (10-fold, $p < 0.01$) CHIKV RNA levels in the serum (Figure 1C) compared with isotype mAb control-treated mice. The reduction of viral RNA in circulation was associated with diminished levels in the spleen and contralateral foot (Figures 1D–1F). However, the ipsilateral foot, which is adjacent to the site of inoculation and should not require viral transport via the blood for infection, did not show statistically significant differences (0.5-fold, $p = 0.08$) in viral RNA levels between anti-GR-1 and isotype mAb-treated mice (Figure 1E).

The first round of alphavirus replication in mammalian hosts is initiated by virus produced in insect cells. Given that distinct N-linked glycans are present on proteins from invertebrate compared to vertebrate cells,[15] and arboviruses displaying high mannose carbohydrates can interact with specific lectin receptors on myeloid cells,[16–18] we measured infection with C6/36 *Aedes albopictus* mosquito cell-passaged CHIKV in the context of Ly6C/Ly6G cell depletion. Like the results with mammalian cell-derived CHIKV, we observed significant reductions in viral RNA levels in the serum, spleen, and contralateral feet of mice inoculated with C6/36 cell-derived virus and treated with anti-GR-1 antibody (Figures S2A, S2B and S2D). We also observed small, yet statistically significant, reductions (3-fold, $p < 0.05$) of CHIKV RNA in the ipsilateral foot (Figure S2C). These data suggest that Ly6C/Ly6G myeloid cells are required for efficient dissemination of both insect cell- and mammalian cell-derived CHIKV.

Depletion of myeloid cells reduces dissemination of multiple alphaviruses

We next determined whether another strain of CHIKV (CHIKV-AF15561 [AF], Thailand) and a second arthritogenic alphavirus, RRV (strain T48), also required Ly6C/Ly6G cells

for early spread. We administered anti-GR-1 or isotype control mAbs to mice 24 h prior to inoculation with CHIKV-AF or RRV by footpad injection and then collected tissues at 18 hpi. When Ly6C/Ly6G cells were depleted, CHIKV-AF (Figures S2E–S2H) and RRV (Figures 1G–1J) also showed reductions of viral RNA levels in serum (10-fold, $p < 0.05$), spleen (10- to 100-fold, $p < 0.01$), and contralateral feet (5-fold, $p < 0.05$). Again, smaller reductions (2-fold, $p < 0.05$) in viral RNA levels were observed in the ipsilateral feet. We confirmed that infectious virus titers also were reduced in these tissues after Ly6C/Ly6G cell depletion (Figures S2I–S2K). Although the effect of Ly6C/Ly6G cell depletion on dissemination was observed with multiple arthritogenic alphaviruses, it was not seen with Zika virus (ZIKV),[19] a mosquito-transmitted flavivirus, suggesting that administration of the anti-GR-1 antibody does not broadly elicit an antiviral response.

We next tested whether Ly6C/Ly6G cell depletion could reduce alphavirus spread to central nervous system tissues. To evaluate this, we administered anti-IFNAR1 blocking antibody to mice via intraperitoneal injection, which facilitates rapid CHIKV spread to the brain.[20,21] PBS- or anti-IFNAR1-treated mice that were administered control or anti-Ly6C/Ly6G-depleting antibodies were then inoculated with CHIKV-LR, and serum and brain tissues were harvested at 2 dpi. Ly6C/Ly6G cell depletion reduced viral RNA levels in the serum and brain of both anti-IFNAR1- and PBS-treated controls (Figures S3C and S3D) and infectious CHIKV levels in the brain of anti-IFNAR1-treated mice (Figure S3E). Thus, Ly6C/Ly6G myeloid cells are required for rapid CHIKV spread to the brain, and this effect appears to be independent of type I IFN signaling.

Effect of myeloid cells on CHIKV dissemination is independent of the alphavirus receptor MXRA8

Global deletion in mice of matrix remodeling-associated protein 8 (MXRA8), a principal arthritogenic alphavirus receptor, results in reduced virus infection and spread.[22] Because dissemination of multiple arthritogenic alphaviruses was affected by anti-GR-1 mAb treatment, we questioned whether myeloid cells facilitate virus spread through interactions with MXRA8. We first confirmed the reduced spread phenotype in *Mxra8*$^{\Delta 8/\Delta 8}$ mice (out-of-frame knockout allele)[23] was recapitulated at early time points post infection. We inoculated age- and sex-matched congenic wild-type (WT) or *Mxra8*$^{\Delta 8/\Delta 8}$ mice. At 18 hpi, we observed significant decreases in viral RNA levels in the serum of *Mxra8*$^{\Delta 8/\Delta 8}$ mice compared to WT controls (Figure S4A). We then performed Ly6C/Ly6G cell depletions and CHIKV infections in *Mxra8*$^{\Delta 8/\Delta 8}$ mice or WT mice. As expected, we saw reduced levels of viral RNA in the serum, spleen, and contralateral foot (Figures S4B, S4C, and S4E), and smaller reductions in the ipsilateral foot (Figure S4D) in anti-GR-1-treated WT animals and isotype control mAb-treated *Mxra8*$^{\Delta 8/\Delta 8}$ mice. In mice that lacked expression of MXRA8 and were depleted of Ly6C/Ly6G cells, we observed an additive effect, as viral RNA levels were reduced even further in all tissues (Figures S4B–S4E). These data suggest that the cell types that mediate MXRA8-dependent effects on virus dissemination are distinct from those targeted by Ly6C/Ly6G depletion.

CHIKV replication in the skin and accumulation in the DLN is impaired by anti-GR-1 antibody

To address whether Ly6C/Ly6G cell depletion affects the earliest phases of infection, we first determined the kinetics of virus replication in the proximal skin and transit to the DLN. We inoculated four cohorts of mice; harvested the skin and DLN (popliteal lymph node [LN]) of one cohort each at 1, 4, 8, or 18 hpi; and analyzed the tissues for CHIKV RNA. After a 4-h lag, viral RNA levels in the skin showed exponential growth indicative of active viral replication with an approximately 10,000-fold increase in viral RNA by 18 hpi (Figure 2A). In the DLN, viral RNA also was detected at 1 hpi, prior to active replication, which presumably is due to direct lymphatic transport (Figure 2B). To determine if the viral RNA present in each site reflects productive infection, we measured the subgenomic:genomic RNA ratio at 18 hpi. Actively replicating alphaviruses produce a 26S subgenomic RNA encoding the structural genes (capsid, E3, E2, 6K, and E1) in excess of the full-length genome[4,24,25] resulting in a ratio above 1. The skin showed a ratio >1 starting at 8 hpi (Figure 2C), whereas the ratio in the DLN remained at ~1 throughout the time course of infection (Figure 2D). Moreover, the subgenomic:genomic RNA ratio in the skin was diminished after anti-GR-1 mAb treatment (Figure 2E). These data suggest the following: (1) at 8 and18 hpi, active viral replication occurs in the skin more than in the DLN; (2) virus levels in the DLN likely reflect replication in the skin and transit via draining lymphatics; and (3) Ly6C/Ly6G cells contribute to active CHIKV replication in the skin.

To begin to determine how Ly6C/Ly6G cells affect virus spread from the skin to the DLN, we treated mice with anti-GR-1 or isotype control mAb, inoculated them subcutaneously via footpad injection, and measured viral RNA in the skin over time (1, 4, 8, or 18 hpi) in different cohorts of animals. Notably, anti-GR-1 treatment resulted in significant decreases in viral RNA levels in the skin at 8 and 18 hpi (5-fold, $p < 0.05$), time points that correspond to the initial and subsequent rounds of replication (Figure 2F). In the DLN, we observed no statistically significant differences in viral RNA levels in anti-GR-1 and isotype control-treated animals at 1, 4, and 8 hpi, but we detected a difference (10-fold, $p < 0.01$) at 18 hpi (Figure 2G), which could reflect disparities in replication in the skin at the preceding time point. Overall, these data show that depletion of Ly6C/Ly6G myeloid cells reduces viral RNA levels in tissues near the site of inoculation at very early time points, which affects viral RNA levels in the DLN.

Accumulation of CHIKV in the medullary sinus and DLN fluid is reduced by anti-GR-1 mAb treatment

Given that anti-GR-1 treatment resulted in a reduction of active viral RNA synthesis in the skin but not in the DLN, we hypothesized that infectious virus levels in DLN fluid also might be affected by Ly6C/Ly6G cell depletion. To test this idea, at 18 hpi, we physically separated the lymphatic fluid from the cellular and matrix compartments of the DLN and measured levels of viral RNA and infectious virus. We observed an approximately 10-fold reduction ($p < 0.01$) in infectious virus in the fluid phase fraction (Figure 3A) as well as the intact DLN (Figure 3B) from mice treated with anti-GR-1 antibody. Similar reductions in viral RNA were detected in intact DLN (Figure 3C). We also determined whether anti-GR1 mAb treatment altered the localization of CHIKV in the DLN using confocal microscopy.

In agreement with previous studies,[26] in isotype control-treated mice, CHIKV antigen, as detected with anti-E1 antibodies, accumulated principally at the periphery of the DLN in the subcapsular and medullary sinuses at the 18-h time point (Figure 3D). Accumulation was reduced in mice treated with anti-GR-1 mAb, with prominent decreases seen in the medullary sinus (Figures 3D–3F). Together, these data demonstrate that depletion of Ly6C/Ly6G cells results in a reduction of CHIKV in the fluid phase, marginal zone, and medullary sinus compartments of the DLN.

Anti-GR-1 mAb administration does not affect lymphatic trafficking of alphaviruses to the DLN

One plausible explanation for the reduced virus accumulation in the setting of depletion of Ly6C/Ly6G myeloid cells is altered trafficking of virus within afferent lymphatics. This hypothesis is possible since neutrophil infiltration of LNs can influence fluid flow dynamics in the context of inflammation.[27] To test this possibility, we first took advantage of a distantly related avian alphavirus in the Western equine encephalitis subcomplex, Aura virus (AURV), which replicates poorly, if at all, in vertebrate cells.[28] In these experiments, AURV serves as a relatively inert alphavirus particle that can be transported by lymphatic fluid to the DLN without actively replicating in the skin. We inoculated isotype control and anti-GR-1-mAb-treated mice with 10^5 focus-forming units (FFU) of AURV, a dose 100-times higher than used in our CHIKV experiments, in anticipation that the virus might be cleared rapidly and difficult to detect because of a lack of replication. We first established that AURV does not actively replicate in the skin or DLN by performing a time course of infection in the skin (Figure 4A) and determining the subgenomic:genomic RNA ratio in the skin and the DLN. In both tissues, AURV RNA had a subgenomic:genomic ratio of ~1, which did not change over time (Figures 4B and 4C). Moreover, at 18 hpi, we observed no effect of Ly6C/Ly6G cell depletion, as levels of AURV RNA were similar in the skin and DLN in isotype and anti-GR-1 mAb treated mice (Figures 4D and 4E). In a set of confirmatory experiments, we utilized an Eilat (EILV)-CHIKV chimeric virus that encodes for EILV non-structural proteins and CHIKV structural proteins.[29] EILV is an insect-specific alphavirus that cannot replicate in mammalian cells.[30] Thus, in insect but not mammalian cells, the chimeric EILV-CHIKV produces alphavirus virions displaying the CHIKV structural proteins. As observed with AURV, viral RNA levels of EILV-CHIKV in the ipsilateral foot skin and DLN at 18 hpi were not affected by anti-GR-1 mAb treatment (Figures 4F and 4G). Together, these data suggest that Ly6C/Ly6G cell depletion does not directly affect lymphatic transport of alphavirus virions. As an additional test, we monitored the effect of Ly6C/Ly6G cell depletion on transit from the skin to the DLN of a 2,000-kDa fluorescein isothiocyanate (FITC)-conjugated dextran. Mice were administered anti-GR-1, inoculated with CHIKV, and, at 8 hpi, administered 40 ng of FITC-dextran in the left rear footpad. DLNs were harvested 4 h later and either imaged by confocal microscopy (Figure 4H) or evaluated for FITC-dextran levels using fluorometry (Figure 4I). We observed no statistically significant differences in accumulation of FITC-dextran in the DLN at 12 hpi in the setting of anti-GR-1 treatment. Together, these data demonstrate that fluid phase trafficking from the skin to the DLN remains intact after Ly6C/Ly6G cell depletion and, thus, is not likely to account for the reductions of CHIKV RNA in the DLN, and that active

virus replication in the skin is required to observe the effect of Ly6C/Ly6G cell depletion on virus dissemination to the DLN.

Ly6C/Ly6G cell depletion affects CHIKV replication in the CD45^{-} non-hematopoietic cell compartment of the skin

The skin proximal to the inoculation site supports replication of CHIKV, and depletion of Ly6C/Ly6G cells reduces viral RNA levels in this compartment (Figure 2). To determine if the reduction of CHIKV infection in the skin after Ly6C/Ly6G cell depletion reflects effects on non-hematopoietic cells, we subcutaneously inoculated isotype- or GR-1-antibody-treated mice in the footpad with 10^5 FFU of a recombinant CHIKV strain expressing a fluorescent reporter protein (CHIKV-AF15561-Venus). At 18 hpi, skin cells were released by enzymatic digestion and incubated with an anti-alphavirus mAb (DC2.112)[31] that recognizes the E1 protein. We performed flow cytometry to analyze CHIKV antigen and YFP expression levels in CD45^{-} cells (Figure S5). Notably, CD45^{-} cells in the skin harvested from anti-GR-1 mAb-treated mice had lower levels of CHIKV antigen (Figures 5A and 5B) and YFP expression (Figures 5A and 5C), suggesting that a reduced number of non-hematopoietic cells were infected in the absence of Ly6C/Ly6G myeloid cells.

To characterize the stromal cell populations that are affected by Ly6C/Ly6G depletion, we performed a more detailed flow cytometry analysis of the skin. Isotype- or anti-GR-1-treated mice were inoculated with CHIKV-AF15561-Venus reporter virus, and skin was harvested at 18 hpi. Staining with antibodies against CD31,[32] E-cadherin,[33] CD29,[4] EpCAM,[34] and Sca-1[34] were used to identify endothelial cells (CD45^{-}CD31^{+}), epithelial cells (CD45^{-}E-cadherin^{+}CD31^{-}), fibroblasts (CD45^{-}CD29^{+}CD31^{-}), and interfollicular epidermal keratinocytes (CD45^{-}EpCAM^{+} Sca-1^{+}CD31^{-}). Compared to isotype-treated control animals, the numbers of YFP^{+} cells were reduced in several stromal cell populations in the skin of Ly6C/Ly6G cell-depleted animals (Figures 5D–5H). This reduction was particularly apparent for endothelial and E-cadherin^{+}CD31^{-} cells (Figures 5D–5F), which had approximately 10-fold reductions in the number of YFP^{+} cells. These data suggest that infiltrating Ly6C/Ly6G myeloid cells facilitate CHIKV infection of multiple non-hematopoietic cell types in the skin.

Monocytes in the skin support CHIKV infection

Given that reduced virus replication in the skin was observed starting at 8 hpi, we evaluated the kinetics of infiltration of Ly6C^{hi} monocytes and Ly6G^{+} neutrophils. Classical monocytes were defined as CD45^{+}CD3^{-}B220^{-}NK1.1^{-}Ly6G^{-}CD11b^{+}CD115^{+}Ly6C^{hi} cells, and neutrophils were defined as CD45^{+}CD3^{-}B220^{-}NK1.1^{-}CD11b^{+}Ly6G^{+} cells (Figure S5). We harvested skin of the ipsilateral foot at 0, 8, or 18 hpi and analyzed cells by flow cytometry. Notably, the number of monocytes in the skin increased by 10-fold between 0 and 8 hpi, and 5-fold further between 8 and 18 hpi, (Figures S6A and S6B) compared to neutrophils, which remained relatively constant over the 18-h time course of infection (Figures S6C and S6D). We also assessed skin-infiltrating monocytes and neutrophils for CHIKV antigen (E1) staining. While both cell types stained positively for CHIKV antigen at 8 hpi (Figures 6A and 6B), the number of CHIKV antigen-positive monocytes increased over time, with ~95% of the cells positive at 18 hpi, whereas the number of E1-positive

neutrophils increased to a much lesser extent (Figures 6A and 6B). As monocytes and neutrophils in the skin stained positively for CHIKV antigen prior to the detection of virus in the blood (Figure 1A), these cells likely acquired viral antigen at the initial site of infection. In contrast, we observed smaller increases in the fraction or number of CHIKV antigen-positive monocytes and neutrophils in the DLN between 8 and 18 hpi (Figures 6C and 6D).

To determine if infiltrating monocytes in the skin were productively infected with CHIKV, we inoculated mice with CHIKV AF15561-Venus, harvested the ipsilateral foot skin and DLN, and evaluated YFP expression by flow cytometry. We harvested tissue at 18 and 36 hpi, with the expectation that there might be a delay in viral replication due to the inherently attenuating effect of inclusion of the Venus reporter gene.[35] At 18 hpi, ~10% of $Ly6C^{hi}$ monocytes in the skin expressed YFP, and this increased to approximately 25% at 36 hpi (Figures 6E and 6F). At the same time point, few, if any, monocytes were productively infected in the DLN. Other myeloid cell subsets, including conventional DCs (cDCs: $CD11c^{+}CD11b^{-}$), monocyte-derived macrophages (Mo-Macs: $F4/80^{+}Ly6C^{+}$), and monocyte-derived DCs (Mo-DCs: $CD11c^{+}CD11b^{+}Ly6C^{+}$) were either negative for YFP expression (cDCs) or positive at lower levels than $Ly6C^{hi}$ monocytes (Mo-Macs and Mo-DCs) (Figures S7A and S7C) in the skin. Moreover, the immune cell infiltrate of the skin during CHIKV infection was largely depleted with anti-GR-1 antibody (Figures S7B and S7D). Collectively, these data suggest that CHIKV infection in $Ly6C^{hi}$ monocytes predominantly occurs in the skin at very early time points after virus inoculation and that monocytes are the principal myeloid cell subset that is productively infected by CHIKV in the skin.

Depletion with anti-Ly6C but not anti-Ly6G antibodies reduces CHIKV infection in the skin and subsequent dissemination

Our flow cytometry data suggested that skin-associated monocytes and not neutrophils might amplify CHIKV infection proximal to the initial infection site. As anti-GR-1 mAb depletes both myeloid cell subsets, we distinguished their roles by performing separate depletions with mAbs against Ly6G (clone 1A8) or Ly6C (clone Monts-1) and assessing effects on viral RNA levels in the skin, DLN, blood, ipsilateral foot, and distal tissues. Depletion of neutrophils (see Figures 7A and S1) alone had no effect on viral burden in any of the tissues assessed compared to isotype-treated controls except for a small (1.5-fold, $p < 0.01$) effect in the DLN (Figures 7B–7G). In contrast, depletion of monocytes (Figures 7A and S1) with anti-Ly6C mAb largely recapitulated the phenotype observed with anti-GR-1 mAb depletion, with significant reductions in viral RNA levels in the skin, DLN, serum, spleen, and contralateral foot but no reduction in the ipsilateral foot (Figures 7H–7M). These results support the idea that $Ly6C^{hi}$ monocytes are the key infiltrating myeloid cell type required for early CHIKV dissemination.

DISCUSSION

Myeloid cells have been reported as vehicles of dissemination for several arboviruses.[13,36,37] In the current study, we demonstrated that, within 18 h of infection, $Ly6C^{hi}$ monocytes

become productively infected in the skin, a time point that precedes virus infection of monocytes in circulation. Depletion of myeloid cells resulted in reduced virus replication in $CD45^{-}$ non-hematopoietic cells in the skin proximal to the site of inoculation and decreased viral RNA levels in the DLN. Lymphatic fluid trafficking of virus or small molecules, however, was not affected by myeloid cell depletion. Instead, the enhanced alphavirus infection in the skin that occurs in the presence of $Ly6C^{+}$ myeloid cells resulted in increased quantities of virus draining to the DLN, which likely enabled dissemination into the blood and to distal tissue sites.

A principal barrier that prevents transport of alphaviruses from the initial infection site in the skin to the local DLN and beyond are LECs.[6,7] $MARCO^{+}$ LECs filter alphaviruses from the afferent lymphatics prior to their entry into the bloodstream.[6] As such, a delicate balance exists between the kinetics of clearance and virus replication. Viruses that replicate to high-titer rapidly[38,39] can disseminate more efficiently in mammalian hosts, and mutants (e.g., CHIKV E2 K200R) that evade interactions with MARCO and LECs enter circulation more rapidly.[40] Our measurement of the subgenomic:genomic ratio of CHIKV RNA in the DLN suggests that, at 18 hpi, much of the viral RNA at this site is not actively replicating. Thus, the DLN may be a “dead-end” site in the dissemination cascade that principally serves to induce adaptive immune responses.[26,41] Nonetheless, the bottleneck imposed by MARCO and LECs can be overcome by transit of a threshold amount of virus that is produced up-stream in the inoculated foot and exceeds the filtering capacity of MARCO and LECs. Alternatively, disabling of innate immune responses in the DLN could facilitate alphavirus replication in myeloid cell subsets and more rapid spread.[12,42]

Non-hematopoietic cells and infiltrating monocytes in the skin appear to act in concert to increase the amount of virus that enters the lymphatics during CHIKV infection. An unexpected observation was that extravasated $Ly6C^{hi}$ monocytes became productively infected at early time points. In contrast, in the blood, monocyte infection by CHIKV and other alphaviruses is limited by type I IFNs that are produced by plasmacytoid DCs (pDCs) and instructed by the microbiome.[12] We also observed that DLN-associated monocytes appear restricted in their ability to replicate virus. Possibly, counter-regulatory local immune responses in the skin (e.g., transforming growth factor [TGF]-β) could paradoxically render monocytes permissive to infection.[43] Alternatively, monocytes may not respond to the dominant IFN (type III, IFN-λ) at epithelial barrier surfaces[44–46] because they lack expression of the IFNLR1 subunit.[47–49] Differences in permissiveness to CHIKV infection of monocytes from blood, DLN, and tissue also could be due to their transcriptional or programmatic differences.[50] It will be important to continue to characterize monocyte subsets and their functions in diverse inflammatory settings, including during virus infections such as CHIKV.

Myeloid cells have been implicated in the early steps of pathogenesis of other arbovirus infections, including the flaviviruses, Dengue virus (DENV), ZIKV, and West Nile virus (WNV).[37,51] These interactions are complex, and multiple targets have been described depending on the virus, timing of analysis, and biological context. One study showed that, at early time points (12–24 hpi) after virus inoculation, DENV replicated in conventional DCs and tissue-resident macrophages in the dermis, with skin-associated monocyte-derived

DCs becoming targets of infection at slightly later time points (48–72 hpi).[51] In human skin explant cultures, Langerhans cells reportedly become infected with DENV, a process that was enhanced by interleukin (IL)-1β produced by keratinocytes.[52] Dermal DCs also have been described as targets of DENV infection in the skin and contributed to the induction of protective $CD4^+$ T cell responses.[53] In our study with CHIKV, monocytes infiltrated into the skin rapidly (within 8 hpi) and became productively infected soon thereafter. We also observed that some Mo-DCs were infected by CHIKV in the skin, although to a much lesser extent than monocytes. Thus, while Mo-DCs likely contribute to virus production in the skin, their permissiveness may become limited as they differentiate into DCs, a phenotype that contrasts with that seen after DENV infection.[51]

Limitations of the study

(1) We did not identify the signals generated by monocytes during CHIKV infection that influence the permissiveness of surrounding stromal populations. It will be important to determine the interactions between monocytes and non-hematopoietic cells that modulate alphavirus infection in the skin and potentially other tissue sites. (2) While we confirmed a requirement for $Ly6C^+$ cells for two strains of CHIKV and RRV, we did not test this mechanism against other arthritogenic (e.g., MAYV and ONNV) or encephalitic alphaviruses. It may be especially interesting to evaluate how $Ly6C^+$ cell depletion affects spread of Eastern equine encephalitis virus, since this alphavirus encodes a microRNA target sequence in its genome that results in attenuated replication in myeloid cells.[54]

In summary, arthritogenic alphaviruses must disseminate from the initial infection site to the circulation to generate high-titer viremia for mosquito transmission. We provide evidence that infiltrating monocytes in the skin can be exploited by arthritogenic alphaviruses to enhance virus production locally and bypass barriers of virus dissemination in the DLN to enable more rapid dissemination to distant sites.

STAR★METHODS

RESOURCE AVAILABILITY

Lead contact—Further information and requests for resources and reagents should be directed to the Lead Contact, Michael S. Diamond (mdiamond@wustl.edu).

Materials availability—All requests for resources and reagents should be directed to the lead contact author. This includes viruses, primer-probe sets, antibodies, and mice. All reagents will be made available on request after completion of a Materials Transfer Agreement (MTA).

Data and code availability—All data supporting the findings of this study are available within the paper and are available from the corresponding author upon request. This paper does not include original code. Any additional information required to reanalyze the data reported in this paper is available from the lead contact upon request.

EXPERIMENTAL MODEL AND STUDY PARTICIPANT DETAILS

Antibodies, cells, and viruses—Anti-Ly6C/Ly6G (GR-1, clone RB6-8C5 Cat# BE0075), anti-Ly6C (Ly6C, clone Monts-1 Cat # BE0203) and anti-Ly6G (Ly6G, clone 1A8 Cat # BP0075-1) antibodies and corresponding isotype control mAbs were purchased from Bio X Cell. Anti-IFNAR1 (clone MAR1-5A3, Cat # I-400) antibody was purchased from Leinco Technologies. Vero cells (CCL-81, ATCC) and BHK-21 [clone 13] cells (CCL-10, ATCC) were cultured in Dulbecco's Modified Eagle Medium (DMEM, Gibco) supplemented with 5% heat-inactivated fetal bovine serum (FBS) at 37°C with 5% CO_2. CHIKV AF15561, AF15561-Venus and CHIKV LR-2006 OPY1, and RRV T48 were generated from infectious cDNA clones and passaged once on BHK-21 cells (RRV), Vero cells (AF15561 and LR-2006), or *Aedes albopictus* C6/36 cells (CRL-1660, ATCC) (LR-2006). AURV[28] was obtained from the World Reference Center for Emerging Viruses and Arboviruses (University of Texas Medical Branch, gift of K. Plante) and was passaged once in chicken embryonic fibroblasts. Chimeric EILV-CHIKV virus was generated as reported previously[29] and obtained from the World Reference Center for Emerging Viruses and Arboviruses (generous gift of S. Weaver).

Mice—Four-week-old, male, C57BL/6J mice were used for all experiments in the study. All mouse experiments were performed according to the Guide for the Care and Use of Laboratory Animals of the National Institutes of Health after approval by the Institutional Animal Care and Use Committee (IACUC) at the Washington University School of Medicine and the University of Colorado School of Medicine. All infections in mice were performed under anesthesia with ketamine hydrochloride (80 mg/kg) and xylazine (15 mg/kg) or isoflurane. C57BL/6J mice were purchased from Jackson Laboratories (Cat # 000664). Congenic *Mxra8*$^{\Delta 8/\Delta 8}$ mice on a C57BL/6J background were generated as described previously.[23]

METHOD DETAILS

Immune cell depletion studies—Individual mice were administered 700 μg of anti-GR-1, anti-Ly6C, or anti-Ly6G or isotype control antibodies as indicated by intraperitoneal injection at 24 h prior to virus infection. Antibodies were diluted in Dulbecco's Phosphate Buffered Saline (DPBS, Gibco). Mice were inoculated in the rear footpad by subcutaneous injection with 10^3 FFU of LR-2006, AF15561, or RRV; or 10^5 FFU of AURV or AF15561-Venus diluted in DPBS. In some experiments, mice were administered anti-GR-1 antibody 24 hpi and sacrificed at 48 hpi. Mice were sacrificed by ketamine overdose and perfused extensively with 20 mL of DPBS. Indicated tissues were harvested and flash frozen on dry ice prior to storage at −80°C. Tissues were thawed and homogenized (ThermoFisher) in 1 mL of DMEM supplemented with 2% FBS.

Quantification of viral RNA or infectious virus particles—For qRT-PCR analysis, viral RNA was extracted from 75 μL of tissue homogenate using a MagMAX-96 Viral RNA Isolation Kit (ThermoFisher) and KingFisher Flex 96-well-plate nucleic acid extraction instrument (ThermoFisher). One-step qRT-PCR was performed using TaqMan RNA-to-CT 1-Step Kit (ThermoFisher). Primer sequences Forward 5′-TCGACGCGCCCTCTTCTTTAA-3′, Reverse 5′-ATCGAATGCACCGCACACT-3',

and probe 5′-5′-/56-FAM/ACCAGCCTG/ZEN/CACCCATTCCTCAGAC/3IABkFQ/−3′ were used for CHIKV-LR E1 structural gene; Forward 5′-AAAGGGCAAACTCAGCTTCAC-3′, Reverse 5′-GCCTGGGCTCATCGTTATTC-3', and probe 5′-/56-FAM/CGCTGTGA/ZEN/CAGTGGTTTCGTGTG/3IABkFQ/-35′ for nsP1 non-structural gene for CHIKV-LR; Forward 5′-TCGACGCGCCATCTTTA-3′, Reverse 5′-ATCGAATGCACCGCAC-3', and probe 5′-/56-FAM/ACCAGCC/ZEN/TGCACCCACTCCTC/3IABkFQ/-3′ for CHIKV-AF E1 structural gene, Forward 5′-CGGATCAAACCTGCACAATTC-3′, Reverse 5′-TTCGTAGGTAAGGCAAGGTATTT-3', and probe 5′-/56-FAM/ATACTCTG/ZEN/CCACCAATGCATGGGA/3IABkFQ/-3′ for AURV E1, and Forward 5′-CCACTGATATCCAACCCGAAG-3′, Reverse 5′-GCCCATTTACTCAGACCTGTAG-3' and probe 5′ 5′-/56-FAM/ACACCAAC/ZEN/ACGATGCAGAACTATCTCC/3IABkFQ/−3′ for AURV nsP3; Forward 5′-GTGTTCTCCGGAGGTAAAGATAG-3', Reverse-5′ TCGCGGCAATAGATGACTAC-3′, and probe 5′-/56-FAM/ACCTGTTTA/ZEN/CCGCAATGGACACCA/3IABkFQ/−3′ for RRV nsP3; Forward 5′-TGGAGCTTCTGTCTGTCACC-3′, Reverse 5′-ACGTACGGAGACGGGATAAC-3′, and probe 5′-/56-FAM TCGCTTGAT/ZEN/TACATC/ACG/TGC/CAG/3IABkFQ/−3′ for EILV-CHIKV E1. RNA isolated from viral stocks was used as a standard curve to determine FFU equivalents and normalized to volume (serum), tissue weights (spleen, skin, and feet), or represented as quantity per DLN. Infectious virus from fluid phase of the draining popliteal lymph node was quantified by plaque assay. Briefly, lymph nodes were harvested and crushed gently to release fluid. Supernatant was clarified of capsular debris and cells by centrifugation (5 min at 12,000 x *g*).

Flow cytometry—Peripheral blood was collected, and erythrocytes were lysed using ACK lysis buffer (Gibco). Skin from the left (ipsilateral) foot was harvested, incubated overnight in Dispase II (Roche, 1:100 v/v) in RPMI (Gibco) for 12 h. Skin then was minced and incubated with 50 μg/mL of Liberase (Roche) and 10 μg/mL DNAse I (Roche) for 45 min at 37°C, and then strained through a 100 μm cell strainer. DLNs were harvested, minced, and incubated with Liberase and DNAse I as described above. Blood leukocytes, skin, or DLN cells were incubated with antibodies against CD45 (clone 30-F11 BD Biosciences, Cat # 564279), B220 (clone RA3-6B2, Biolegend, Cat # 103251), CD3 (clone 145-2C11, Biolegend, Cat # 100336), NK1.1 (clone S17016D, Biolegend, Cat # 156514), Ly6G (clone 1A8, Biolegend, Cat # 127616), CD11b (clone M1/70, Biolegend, Cat # 101256), CD115 (clone AFS98, Biolegend, Cat # 135532), Ly6B (clone 7/4, Abcam, Cat # ab53457), Ly6C (clone HK 1.4, Biolegend, Cat # 128016), CD31 (clone 390, Biolegend, Cat# 102430), E-cadherin (clone DECMA-1, Biolegend, Cat# 147310), EpCAM (clone G8.8, Biolegend, Cat# 118206), Sca-1 (Ly6A/E) (clone D7, Biolegend, Cat# 108126), CD29 (clone HMβ1-1), Biolegend, Cat# 102218), eFluor 506 fixable viability dye (Invitrogen, Cat # 65086614), TruStain FcX^{tm} anti-mouse CD16/32 (clone 93, Biolegend, Cat # 101320) and fluorescently labelled (ThermoFisher, Cat # 120186) human anti-E1 antibody, DC2.112[31]. Cells were fixed in 4% paraformaldehyde (PFA) and processed on a LSRFortessa BD X-20 flow cytometer. Data were analyzed on FlowJo software, (BD Biosciences, version 10.8.1).

Lymph node staining and imaging—DLNs were oriented to cut a cross-section through the subcapsular to medullary sinus, embedded in Optimal Tissue Cutting medium (EMS Biosciences) and flash frozen in dry-ice cooled isopentane. Frozen sections (16 μm thick) were blocked with 5% donkey and bovine serum and then stained with the following Abs: CHK-166 N297Q (anti-E1),[55–57] ERTR7 (clone ER-TR7, BioRad, Cat # MCA2402), and CD169 (clone 3D6.112, Biolegend, Cat # 142406). Sections were incubated with anti-human secondary antibody (1:200 polyclonal, Jackson ImmunoResearch, Cat# 109-035-003), and images were acquired on a Stellaris confocal microscope with TauSeparation enabled using identical PMT (photomutiplier tube) and laser settings between samples. Images were processed, analyzed, and quantitated using Imaris software 8.0 (Oxford Instruments). For image quantitation, surfaces were created for CHIKV fluorescence using the Imaris automated surfaces function with the same creation parameters for each sample. The total volume and the sum of fluorescence within the created surfaces were calculated using all surfaces in each section.

Lymphatic transport assays—To evaluate lymphatic transport from the skin to the DLN during viral infection, wild-type C57BL/6 mice were first treated with 700 μg of IgG2b isotype control Ab or anti-GR-1 mAb by intraperitoneal injection one day prior to inoculation in the left rear footpad of 10^3 PFU CHIKV LR2006-OPY1. At 8 hpi, mice were inoculated in the left rear footpad with 2 μL of 20 mg/mL FITC-dextran (2,000 kD molecular weight) (Sigma Cat # FD2000S) in PBS based on published methods for measurement of lymphatic vessel diameter.[58] The left draining popliteal lymph node was collected 10 min post FITC-dextran inoculation and fixed in 1 mL of phosphate buffer containing 0.1 M L-lysine, 2% paraformaldehyde (PFA), and 2.1 mg/mL $NAIO_4$ at pH 7.4 for 24 h at 4°C, followed by incubation in 30% sucrose in PBS for 48 h. DLNs were then oriented using a Leica M50 stereo microscope (Leica Microsystems), embedded in OCT compound (Sakura Biosciences), and frozen in dry-ice-cooled isopentane. Sections (16 μm thick) were cut on a Leica cryostat (Leica Microsystems). Slides were counterstained with 300 nM of DAPI (Thermo Fisher) and imaged using a Zeiss LSM780 confocal microscope (Zeiss Microscopy). Confocal microscopy images were collected over the entire popliteal lymph node, and individual fields (tiles) were merged into a single image file using the stitch function in the Zen software (Zeiss Microscopy). Images were analyzed using the open-source software, FIJI (ImageJ2). For quantitative assessment of lymphatic transport,[58] the DLN was collected in 200 μL of PBS, gently homogenized in a Biomasher II tissue homogenizer (Kimble-Chase) and fixed with 200 μL of 2% PFA in PBS. Fluorescence intensity for each sample was determined using a Tecan Infinite 200 Pro plate reader. Fluorescence intensities for DLNs were normalized per sample by subtracting signal from the corresponding cervical LN, and then absolute quantity of FITC-dextran present in each DLN was calculated based on a standard curve of fluorescence intensity versus FITC-dextran concentration.

QUANTIFICATION AND STATISTICAL ANALYSIS

Statistical significance was assigned when p values were <0.05 using Prism version v 10.1.2 (GraphPad). Tests, number of animals (n), mean values, and statistical comparison groups are indicated in the Figure legends.

Supplementary Material

Refer to Web version on PubMed Central for supplementary material.

ACKNOWLEDGMENTS

We would like to thank Deborah Lenschow, Jacco Boon, and Larissa Thackray for technical and conceptual suggestions. This study was supported by NIH grants R01 AI114816, R01 AI123348, R01 AI143673, and R01 AI148144. A.C.H. is supported by a Hanna H. Gray post-doctoral fellowship from the Howard Hughes Medical Institute, GT15172. M.E.B. and H.D.H. are supported by the Division of Intramural Research, NIAID, NIH. Chimeric EILV-CHIKV was provided generously by Scott Weaver at the University of Texas Medical Branch and the World Reference Center for Emerging Viruses and Arboviruses (NIH R24 AI120942).

DECLARATION OF INTERESTS

M.S.D. is a consultant or member of a Scientific Advisory Board for Inbios, Vir Biotechnology, IntegerBio, Merck, GlaxoSmithKline, Akagera Medicines, and Moderna. The Diamond laboratory has received unrelated funding support in sponsored research agreements from Emergent BioSolutions, Moderna, IntegerBio, and Vir Biotechnology.

REFERENCES

1. Weaver SC, and Forrester NL (2015). Chikungunya: Evolutionary history and recent epidemic spread. Antiviral Res 120, 32–39. 10.1016/j.antiviral.2015.04.016. [PubMed: 25979669]
2. Amaral JK, Bilsborrow JB, and Schoen RT (2020). Chronic Chikungunya Arthritis and Rheumatoid Arthritis: What They Have in Common. AmAm. J. Med 133, e91–e97. 10.1016/j.amjmed.2019.10.005.
3. Silva LA, and Dermody TS (2017). Chikungunya virus: epidemiology, replication, disease mechanisms, and prospective intervention strategies. J. Clin. Invest 127, 737–749. 10.1172/JCI84417. [PubMed: 28248203]
4. Young AR, Locke MC, Cook LE, Hiller BE, Zhang R, Hedberg ML, Monte KJ, Veis DJ, Diamond MS, and Lenschow DJ (2019). Dermal and muscle fibroblasts and skeletal myofibers survive chikungunya virus infection and harbor persistent RNA. PLoS Pathog. 15, e1007993. 10.1371/journal.ppat.1007993. [PubMed: 31465513]
5. Tharmarajah K, Everest-Dass A, Vider J, Liu X, Freitas JR, Mosta-favi H, Bettadapura J, von Itzstein M, West NP, Taylor A, et al. (2022). N-Linked Glycans Shape Skin Immune Responses during Arthritis and Myositis after Intradermal Infection with Ross River Virus. J. Virol 96, e0099922. 10.1128/jvi.00999-22. [PubMed: 36000846]
6. Carpentier KS, Sheridan RM, Lucas CJ, Davenport BJ, Li FS, Lucas ED, McCarthy MK, Reynoso GV, May NA, Tamburini BAJ, et al. (2021). MARCO(+) lymphatic endothelial cells sequester arthritogenic alphaviruses to limit viremia and viral dissemination. EMBO J. 40, e108966. 10.15252/embj.2021108966. [PubMed: 34618370]
7. Li FS, Carpentier KS, Hawman DW, Lucas CJ, Ander SE, Feld-mann H, and Morrison TE (2023). Species-specific MARCO-alphavirus interactions dictate chikungunya virus viremia. Cell Rep. 42, 112418. 10.1016/j.celrep.2023.112418. [PubMed: 37083332]
8. Pingen M, Bryden SR, Pondeville E, Schnettler E, Kohl A, Merits A, Fazakerley JK, Graham GJ, and McKimmie CS (2016). Host Inflammatory Response to Mosquito Bites Enhances the Severity of Arbovirus Infection. Immunity 44, 1455–1469. 10.1016/j.immuni.2016.06.002. [PubMed: 27332734]
9. Haist KC, Burrack KS, Davenport BJ, and Morrison TE (2017). Inflammatory monocytes mediate control of acute alphavirus infection in mice. PLoS Pathog. 13, e1006748. 10.1371/journal.ppat.1006748. [PubMed: 29244871]
10. Her Z, Malleret B, Chan M, Ong EKS, Wong SC, Kwek DJC, Tolou H, Lin RTP, Tambyah PA, Rénia L, and Ng LFP (2010). Active infection of human blood monocytes by Chikungunya virus triggers an innate immune response. JJ. Immunol 184, 5903–5913. 10.4049/jimmunol.0904181.

11. Danillo Lucas Alves E, and Benedito Antonio Lopes da F (2018). Characterization of the immune response following in vitro mayaro and chikungunya viruses (Alphavirus, Togaviridae) infection of mononuclear cells. Virus Res. 256, 166–173. 10.1016/j.virusres.2018.08.011. [PubMed: 30145137]
12. Winkler ES, Shrihari S, Hykes BL Jr., Handley SA, Andhey PS, Huang YJS, Swain A, Droit L, Chebrolu KK, Mack M, et al. (2020). The Intestinal Microbiome Restricts Alphavirus Infection and Dissemination through a Bile Acid-Type I IFN Signaling Axis. Cell 182, 901–918.e18. 10.1016/j.cell.2020.06.029. [PubMed: 32668198]
13. Nikitina E, Larionova I, Choinzonov E, and Kzhyshkowska J (2018). Monocytes and Macrophages as Viral Targets and Reservoirs. Int. J. Mol. Sci 19, 2821. 10.3390/ijms19092821. [PubMed: 30231586]
14. Egan CE, Sukhumavasi W, Bierly AL, and Denkers EY (2008). Understanding the multiple functions of Gr-1(+) cell subpopulations during microbial infection. Immunol. Res 40, 35–48. 10.1007/s12026-007-0061-8. [PubMed: 18193362]
15. Zhu F, Li D, and Chen K (2019). Structures and functions of invertebrate glycosylation. Open Biol 9, 180232. 10.1098/rsob.180232. [PubMed: 30958118]
16. Long KM, Whitmore AC, Ferris MT, Sempowski GD, McGee C, Trollinger B, Gunn B, and Heise MT (2013). Dendritic cell immunore-ceptor regulates Chikungunya virus pathogenesis in mice. J. Virol 87, 5697–5706. 10.1128/JVI.01611-12JVI.01611-12. [PubMed: 23487448]
17. Rogers KM, and Heise M (2009). Modulation of cellular tropism and innate antiviral response by viral glycans. J. Innate Immun 1, 405–412. 10.1159/000226422. [PubMed: 20375598]
18. Holmes AC, Basore K, Fremont DH, and Diamond MS (2020). A molecular understanding of alphavirus entry. PLoS Pathog. 16, e1008876. 10.1371/journal.ppat.1008876. [PubMed: 33091085]
19. Reynoso GV, Gordon DN, Kalia A, Aguilar CC, Malo CS, Alesh-nick M, Dowd KA, Cherry CR, Shannon JP, Vrba SM, et al. (2023). Zika virus spreads through infection of lymph node-resident macrophages. Cell Rep. 42, 112126. 10.1016/j.celrep.2023.112126. [PubMed: 36795561]
20. Suzuki Y (2023). Interferon-induced restriction of Chikungunya virus infection. Antiviral Res 210, 105487. 10.1016/j.antiviral.2022.105487. [PubMed: 36657882]
21. Locke MC, Fox LE, Dunlap BF, Young AR, Monte K, and Lenschow DJ (2022). Interferon Alpha, but Not Interferon Beta, Acts Early To Control Chronic Chikungunya Virus Pathogenesis. J. Virol 96, e0114321. 10.1128/JVI.01143-21. [PubMed: 34668781]
22. Zhang R, Kim AS, Fox JM, Nair S, Basore K, Klimstra WB, Rimkunas R, Fong RH, Lin H, Poddar S, et al. (2018). Mxra8 is a receptor for multiple arthritogenic alphaviruses. Nature 557, 570–574. 10.1038/s41586-018-0121-3. [PubMed: 29769725]
23. Zhang R, Earnest JT, Kim AS, Winkler ES, Desai P, Adams LJ, Hu G, Bullock C, Gold B, Cherry S, and Diamond MS (2019). Expression of the Mxra8 Receptor Promotes Alphavirus Infection and Pathogenesis in Mice and Drosophila. Cell Rep. 28, 2647–2658.e5. 10.1016/j.celrep.2019.07.105. [PubMed: 31484075]
24. Ou JH, Rice CM, Dalgarno L, Strauss EG, and Strauss JH (1982). Sequence studies of several alphavirus genomic RNAs in the region containing the start of the subgenomic RNA. Proc. Natl. Acad. Sci. USA 79, 5235–5239. 10.1073/pnas.79.17.5235. [PubMed: 6291034]
25. Fox JM, Huang L, Tahan S, Powell LA, Crowe JE Jr., Wang D, and Diamond MS (2020). A cross-reactive antibody protects against Ross River virus musculoskeletal disease despite rapid neutralization escape in mice. PLoS Pathog. 16, e1008743. 10.1371/journal.ppat.1008743. [PubMed: 32760128]
26. McCarthy MK, Reynoso GV, Winkler ES, Mack M, Diamond MS, Hickman HD, and Morrison TE (2020). MyD88-dependent influx of monocytes and neutrophils impairs lymph node B cell responses to chikungunya virus infection via Irf5, Nos2 and Nox2. PLoS Pathog. 16, e1008292. 10.1371/journal.ppat.1008292. [PubMed: 31999809]
27. Stephens M, and Liao S (2018). Neutrophil-lymphatic interactions during acute and chronic disease. Cell Tissue Res. 371, 599–606. 10.1007/s00441-017-2779-5. [PubMed: 29423716]
28. Toribio R, Diaz-Lopez I, Berlanga JJ, Molina-Jimenez F, Majano P, and Ventoso I (2020). Naturally Occurring and Engineered Alphaviruses Sensitive to Double-Stranded-RNA-Activated

Protein Kinase Show Restricted Translation in Mammalian Cells, Increased Sensitivity to Interferon, and Marked Oncotropism. J. Virol 94, 10–1128. 10.1128/JVI.01630-19.

29. Erasmus JH, Auguste AJ, Kaelber JT, Luo H, Rossi SL, Fenton K, Leal G, Kim DY, Chiu W, Wang T, et al. (2017). A chikungunya fever vaccine utilizing an insect-specific virus platform. Nat. Med 23, 192–199. 10.1038/nm.4253. [PubMed: 27991917]
30. Nasar F, Gorchakov RV, Tesh RB, and Weaver SC (2015). Eilat virus host range restriction is present at multiple levels of the virus life cycle. J. Virol 89, 1404–1418. 10.1128/JVI.01856-14. [PubMed: 25392227]
31. Kim AS, Kafai NM, Winkler ES, Gilliland TC Jr., Cottle EL, Earnest JT, Jethva PN, Kaplonek P, Shah AP, Fong RH, et al. (2021). Pan-protective anti-alphavirus human antibodies target a conserved E1 protein epitope. Cell 184, 4414–4429.e19. 10.1016/j.cell.2021.07.006. [PubMed: 34416146]
32. Lertkiatmongkol P, Liao D, Mei H, Hu Y, and Newman PJ (2016). Endothelial functions of platelet/endothelial cell adhesion molecule-1 (CD31). Curr. Opin. Hematol 23, 253–259. 10.1097/MOH.0000000000000239. [PubMed: 27055047]
33. Young P, Boussadia O, Halfter H, Grose R, Berger P, Leone DP, Robenek H, Charnay P, Kemler R, and Suter U (2003). E-cadherin controls adherens junctions in the epidermis and the renewal of hair follicles. EMBO J. 22, 5723–5733. 10.1093/emboj/cdg560. [PubMed: 14592971]
34. Lou F, Sun Y, and Wang H (2020). Protocol for Flow Cytometric Detection of Immune Cell Infiltration in the Epidermis and Dermis of a Psoriasis Mouse Model. STAR Protoc 1, 100115. 10.1016/j.xpro.2020.100115. [PubMed: 33377011]
35. Jose J, Taylor AB, and Kuhn RJ (2017). Spatial and Temporal Analysis of Alphavirus Replication and Assembly in Mammalian and Mosquito Cells. mBio 8, e02294–16. 10.1128/mBio.02294-16. [PubMed: 28196962]
36. Paul AM, Acharya D, Duty L, Thompson EA, Le L, Stokic DS, Leis AA, and Bai F (2017). Osteopontin facilitates West Nile virus neuro-invasion via neutrophil “Trojan horse” transport. Sci. Rep 7, 4722. 10.1038/s41598-017-04839-7. [PubMed: 28680095]
37. Muralidharan A, and Reid SP (2021). Complex Roles of Neutrophils during Arboviral Infections. Cells 10. 10.3390/cells10061324.
38. Nygaard RM, Lahti L, Boehme KW, Ikizler M, Doyle JD, Dermody TS, and Schiff LA (2013). Genetic determinants of reovirus pathogenesis in a murine model of respiratory infection. J. Virol 87, 9279–9289. 10.1128/JVI.00182-13. [PubMed: 23760238]
39. Roberts A, Deming D, Paddock CD, Cheng A, Yount B, Vogel L, Herman BD, Sheahan T, Heise M, Genrich GL, et al. (2007). A mouse-adapted SARS-coronavirus causes disease and mortality in BALB/c mice. PLoS Pathog. 3, e5. 10.1371/journal.ppat.0030005. [PubMed: 17222058]
40. Carpentier KS, Davenport BJ, Haist KC, McCarthy MK, May NA, Robison A, Ruckert C, Ebel GD, and Morrison TE (2019). Discrete viral E2 lysine residues and scavenger receptor MARCO are required for clearance of circulating alphaviruses. Elife 8, e49163. 10.7554/eLife.49163. [PubMed: 31596239]
41. Davenport BJ, Bullock C, McCarthy MK, Hawman DW, Murphy KM, Kedl RM, Diamond MS, and Morrison TE (2020). Chikungunya Virus Evades Antiviral CD8(+) T Cell Responses To Establish Persistent Infection in Joint-Associated Tissues. J. Virol 94, e02036–19. 10.1128/JVI.02036-19. [PubMed: 32102875]
42. Ryman KD, Klimstra WB, Nguyen KB, Biron CA, and Johnston RE (2000). Alpha/beta interferon protects adult mice from fatal Sindbis virus infection and is an important determinant of cell and tissue tropism. J. Virol 74, 3366–3378. 10.1128/jvi.74.7.3366-3378.2000. [PubMed: 10708454]
43. Liarte S, Bernabe-Garcia A, and Nicolas FJ (2020). Role of TGF-beta in Skin Chronic Wounds: A Keratinocyte Perspective. Cells 9. 10.3390/cells9020306.
44. Hermant P, and Michiels T (2014). Interferon-lambda in the context of viral infections: production, response and therapeutic implications. J. Innate Immun 6, 563–574. 10.1159/000360084. [PubMed: 24751921]
45. Sommereyns C, Paul S, Staeheli P, and Michiels T (2008). IFN-lambda (IFN-lambda) is expressed in a tissue-dependent fashion and primarily acts on epithelial cells in vivo. PLoS Pathog. 4, e1000017. 10.1371/journal.ppat.1000017. [PubMed: 18369468]

46. Wells AI, and Coyne CB (2018). Type III Interferons in Antiviral Defenses at Barrier Surfaces. Trends Immunol. 39, 848–858. 10.1016/j.it.2018.08.008. [PubMed: 30219309]
47. Dickensheets H, Sheikh F, Park O, Gao B, and Donnelly RP (2013). Interferon-lambda (IFN-lambda) induces signal transduction and gene expression in human hepatocytes, but not in lymphocytes or monocytes. J. Leukoc. Biol 93, 377–385. 10.1189/jlb.0812395. [PubMed: 23258595]
48. Read SA, Wijaya R, Ramezani-Moghadam M, Tay E, Schibeci S, Liddle C, Lam VWT, Yuen L, Douglas MW, Booth D, et al. (2019). Macrophage Coordination of the Interferon Lambda Immune Response. Front. Immunol 10, 2674. 10.3389/fimmu.2019.02674. [PubMed: 31798594]
49. Mallampalli RK, Adair J, Elhance A, Farkas D, Chafin L, Long ME, De M, Mora AL, Rojas M, Peters V, et al. (2021). Interferon Lambda Signaling in Macrophages Is Necessary for the Antiviral Response to Influenza. Front. Immunol 12, 735576. 10.3389/fimmu.2021.735576. [PubMed: 34899695]
50. Jakubzick C, Gautier EL, Gibbings SL, Sojka DK, Schlitzer A, Johnson TE, Ivanov S, Duan Q, Bala S, Condon T, et al. (2013). Minimal differentiation of classical monocytes as they survey steady-state tissues and transport antigen to lymph nodes. Immunity 39, 599–610. 10.1016/j.immuni.2013.08.007. [PubMed: 24012416]
51. Schmid MA, and Harris E (2014). Monocyte recruitment to the dermis and differentiation to dendritic cells increases the targets for dengue virus replication. PLoS Pathog. 10, e1004541. 10.1371/journal.ppat.1004541. [PubMed: 25474197]
52. Duangkhae P, Erdos G, Ryman KD, Watkins SC, Falo LD Jr., Marques ETA Jr., and Barratt-Boyes SM (2018). Interplay between Keratinocytes and Myeloid Cells Drives Dengue Virus Spread in Human Skin. J. Invest. Dermatol 138, 618–626. 10.1016/j.jid.2017.10.018. [PubMed: 29106931]
53. Cerny D, Haniffa M, Shin A, Bigliardi P, Tan BK, Lee B, Poidinger M, Tan EY, Ginhoux F, and Fink K (2014). Selective susceptibility of human skin antigen presenting cells to productive dengue virus infection. PLoS Pathog. 10, e1004548. 10.1371/journal.ppat.1004548. [PubMed: 25474532]
54. Trobaugh DW, Gardner CL, Sun C, Haddow AD, Wang E, Chap-nik E, Mildner A, Weaver SC, Ryman KD, and Klimstra WB (2014). RNA viruses can hijack vertebrate microRNAs to suppress innate immunity. Nature 506, 245–248. 10.1038/nature12869. [PubMed: 24352241]
55. Pal P, Fox JM, Hawman DW, Huang YJS, Messaoudi I, Krekly-wich C, Denton M, Legasse AW, Smith PP, Johnson S, et al. (2014). Chikungunya viruses that escape monoclonal antibody therapy are clinically attenuated, stable, and not purified in mosquitoes. J. Virol 88, 8213–8226. 10.1128/JVI.01032-14. [PubMed: 24829346]
56. Fox JM, Roy V, Gunn BM, Huang L, Edeling MA, Mack M, Fremont DH, Doranz BJ, Johnson S, Alter G, and Diamond MS (2019). Optimal therapeutic activity of monoclonal antibodies against chikungunya virus requires Fc-FcgammaR interaction on monocytes. Sci. Immunol 4. 10.1126/sciimmunol.aav5062.
57. Pal P, Dowd KA, Brien JD, Edeling MA, Gorlatov S, Johnson S, Lee I, Akahata W, Nabel GJ, Richter MKS, et al. (2013). Development of a highly protective combination monoclonal antibody therapy against Chikungunya virus. PLoS Pathog. 9, e1003312. 10.1371/journal.ppat.1003312. [PubMed: 23637602]
58. Silva M, Kato Y, Melo MB, Phung I, Freeman BL, Li Z, Roh K, Van Wijnbergen JW, Watkins H, Enemuo CA, et al. (2021). A particulate saponin/TLR agonist vaccine adjuvant alters lymph flow and modulates adaptive immunity. Sci Immunol 6, eabf1152. 10.1126/sciimmunol.abf1152. [PubMed: 34860581]

Highlights

- Skin-associated monocytes are required for efficient CHIKV and RRV dissemination
- Skin-associated infiltrating monocytes are targets of CHIKV infection
- Monocytes promote CHIKV replication in non-hematopoietic cells of the skin
- Lymph node monocytes are not permissive to CHIKV infection

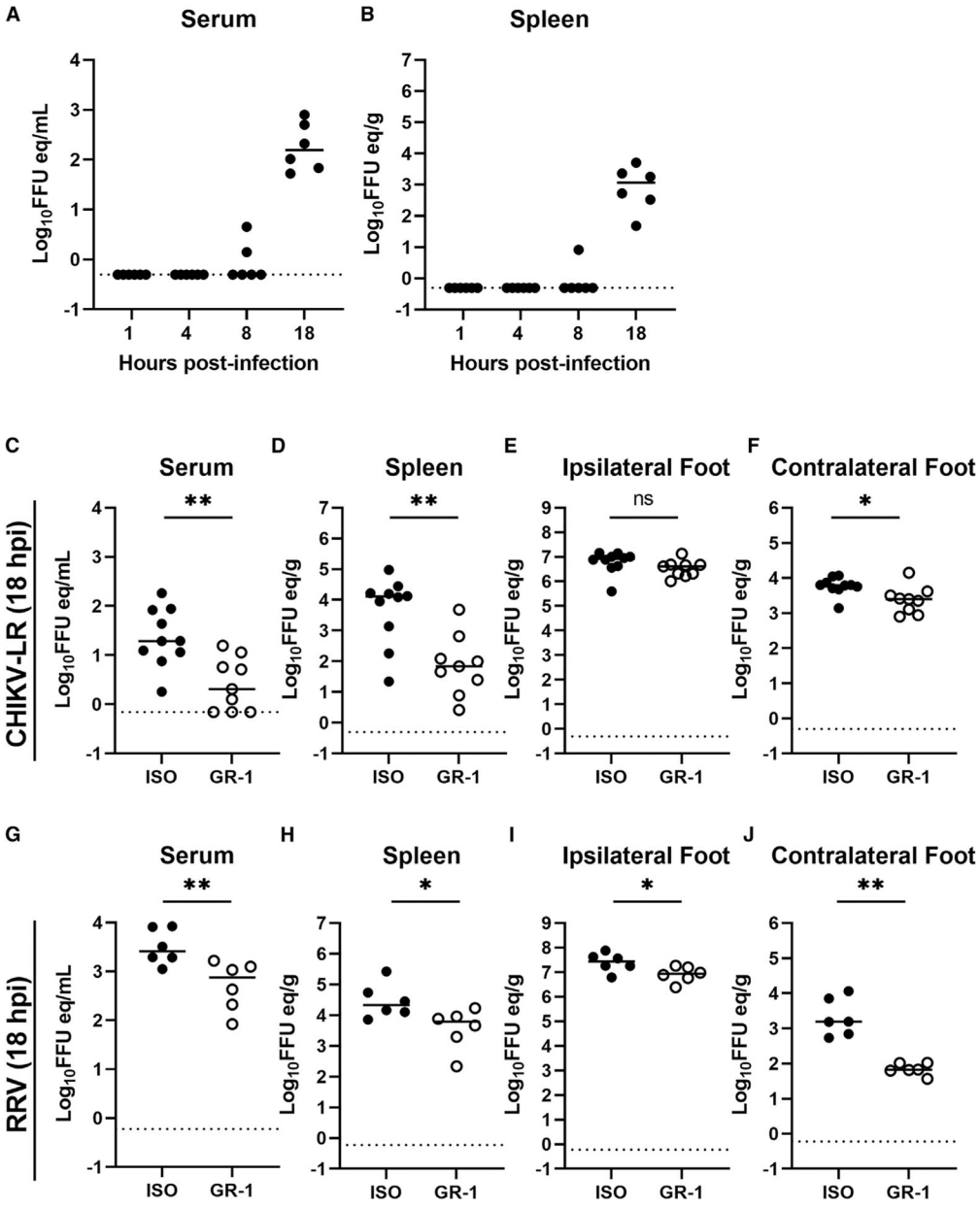

Figure 1. Depletion of myeloid cells reduces CHIKV dissemination

(A and B) Cohorts of 4-week-old male C57BL/6J mice were inoculated with 10^3 FFU of CHIKV (strain La Reunion [LR]-2006) in the left rear footpad. Animals were sacrificed at either 1, 4, 8, or 18 hpi, and viral RNA was quantified by qRT-PCR from serum and spleen (n = 6, two experiments).

(C–J) Mice were administered anti-GR-1 or isotype control antibody via intraperitoneal injection 24 h prior to inoculation with CHIKV-LR (C–F) or RRV (strain T48) (G–J) in the left rear footpad (ipsilateral foot). Serum and indicated tissues were harvested at 18 hpi, and viral RNA was quantified (n = 6–10, two or three experiments). Values in each panel are shown as FFU equivalents (eq) normalized to volume of serum or tissue weight. Bars

indicate median values. Statistical analysis: (C–J) Mann-Whitney test; ns, not significant, *$p < 0.05$, **$p < 0.01$. See also Figures S1–S4.

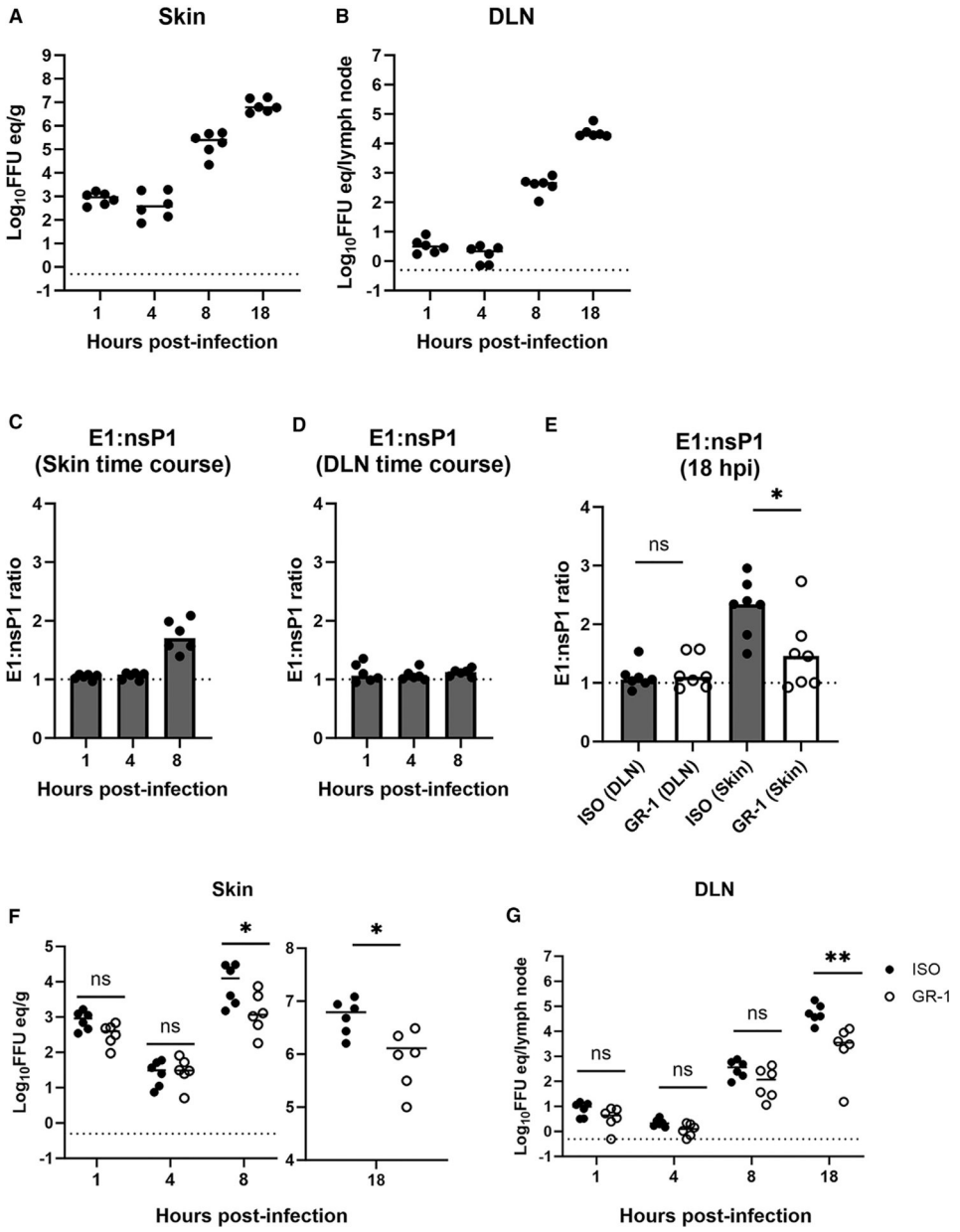

Figure 2. CHIKV replication in the skin and accumulation in the DLN is impaired by anti-GR-1 antibody

(A and B) Cohorts of 4-week-old male C57BL/6J mice were inoculated with CHIKV-LR in the left rear footpad and animals were sacrificed at 1, 4, or 8 hpi. Ipsilateral foot skin and DLNs were collected at each time point, and viral RNA was quantified by qRT-PCR (n = 6, two experiments).

(C and D) Three cohorts of mice were inoculated with CHIKV-LR and sacrificed at 1, 4, and 8 hpi foot skin and DLN were harvested and the levels of subgenomic (*E1* probe) and genomic (*nsp1* probe) RNA were measured and a (*E1*:*nsp1*) ratio was generated (n = 6, two experiments).

(E) Mice pre-treated (day −1) with anti-GR-1 or isotype control antibody were inoculated with CHIKV and sacrificed at 18 hpi, and *E1*:*nsP1* RNA ratios were generated for ipsilateral foot skin and DLN (n = 7, two experiments).

(F and G) Mice were treated with anti-GR1 or isotype control mAb and inoculated with CHIKV as described in (E). At 1, 4, 8, or 18 hpi, ipsilateral foot skin and DLN were harvested, and viral RNA levels (*E1* probe) were determined (n = 6, two experiments). Bars indicate median values. Statistical analysis: (C–E) Mann-Whitney test (comparisons made between anti-GR1 and isotype controls), ns, not significant, *$p < 0.05$, **$p < 0.01$. See also Figure S1.

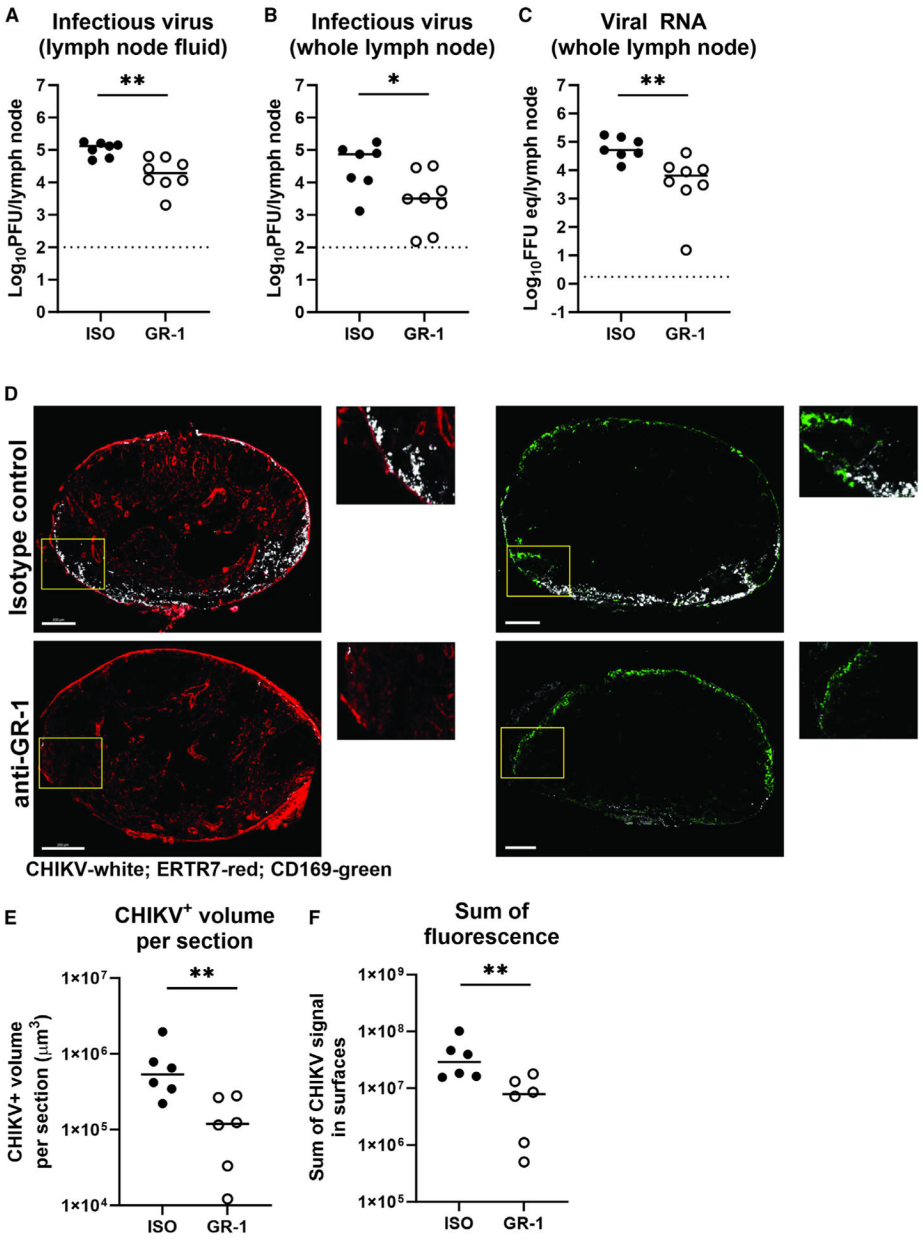

Figure 3. Virus accumulation in the medullary sinus and fluid phase of the DLN is reduced after anti-GR-1 treatment

(Four-week-old male C57BL/6J mice pre-treated (day −1) with anti-GR-1 or isotype control antibody were inoculated in the footpad with 10^3 FFU of CHIKV-LR.

(A) DLNs were harvested, and lymphatic fluid was collected. After clarification by centrifugation, a plaque assay was used to quantify infectious virus (n = 6–7, two experiments). (B and C) DLNs were harvested, and tissue homogenates were assessed for infectious virus by plaque assay (B) and viral RNA (C) (n = 6–7, two experiments). (D) Popliteal DLNs were harvested at 18 hpi, fixed, incubated in 30% sucrose for 48 h, cryo-sectioned, and then stained with the following antibodies: anti-CHIKV E1 (CHK-166 N297Q, white), anti-ERTR7 (red), and anti-CD169 (green). Sections were imaged using confocal microscopy and representative DLNs are shown (n = 6, two experiments). Scale

bars, 200 μm. Boxed insets denote areas of CHIKV-positive cells. Images are representative of two experiments (n = 6). (E and F) Microscopic images of entire DLN were quantitated using automated image processing software to determine the total volume with detectable CHIKV fluorescence (after anti-CHIKV E1 staining) and the total fluorescent signal per section (n = 6–7, two experiments). Bars indicate median values. Statistical analysis: (A–C, E, and F) Mann-Whitney test, *$p < 0.05$, **$p < 0.01$. See also Figure S1.

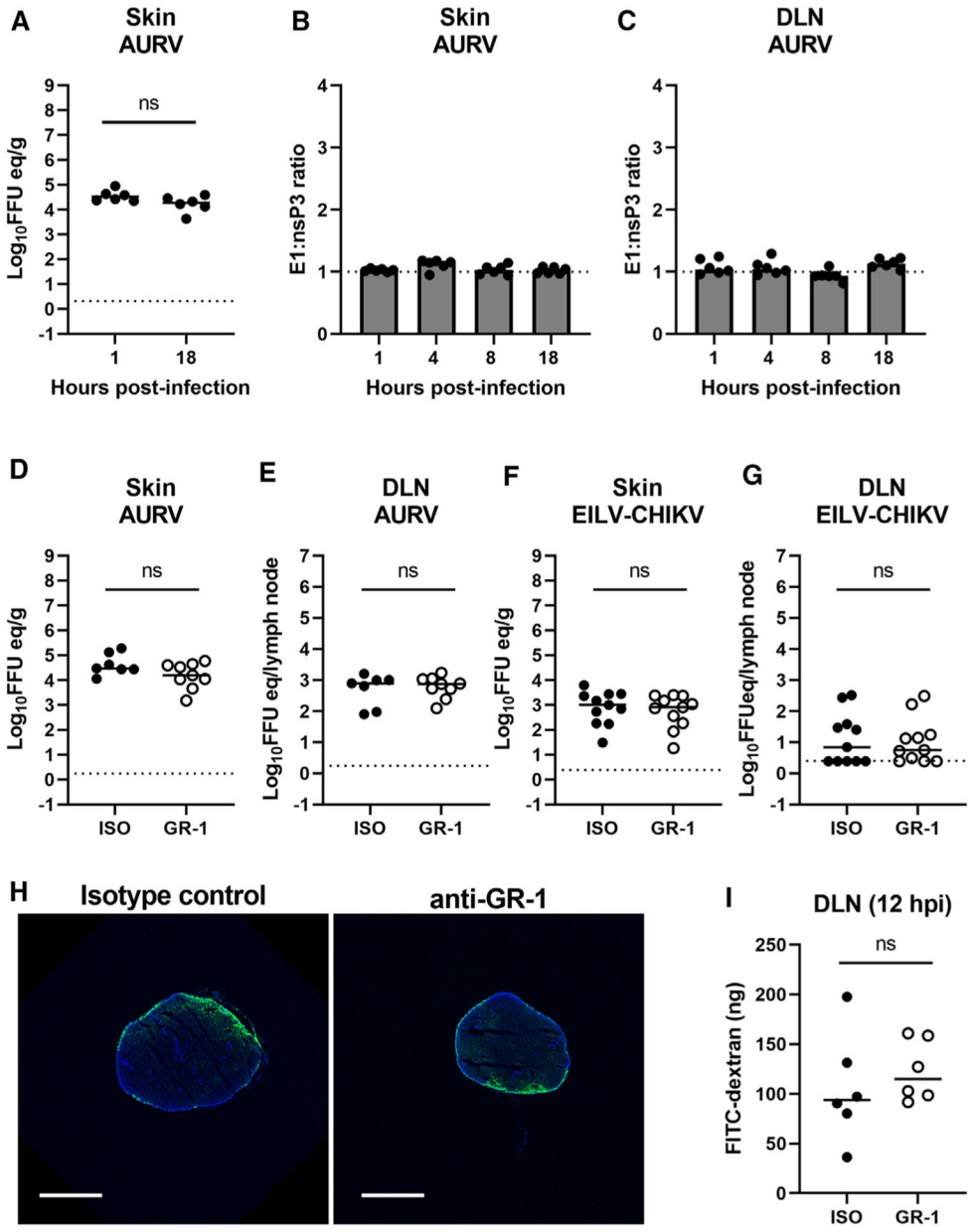

Figure 4. Anti-GR-1 mAb administration does not affect trafficking to the DLN of non-replicating alphaviruses

(A) Four-week-old male C57BL/6J mice were inoculated in the footpad with 10^5 FFU of AURV and harvested at 1 or 18 hpi. Ipsilateral foot skin was collected and assessed for levels of viral RNA.

(B and C) Mice were inoculated in the footpad with 10^5 FFU of AURV and harvested at 1, 4, 8, or 18 hpi. Ipsilateral foot skin (B) and DLN (C) were collected at each time point, and the levels of subgenomic (*E1* probe) (shown alone in A) and genomic (*nsp3* probe) RNA were measured, and a ratio (*E1*:*nsp3*) was generated (n = 6, two experiments).

(D–G) Mice pre-treated (day −1) with anti-GR-1 or isotype control antibody were inoculated with 10^5 FFU of AURV (D and E) or 10^5 FFU of EILV-CHIKV (CHIKV strain 99659) (F and G), and tissues were harvested at 18 hpi. The levels of viral RNA (*E1* probe) were

measured and normalized per weight of tissue or per lymph node (D and E: n = 7 or 9, two experiments. F and G: n = 11, three experiments).

(H and I) Anti-GR-1 or isotype control-treated mice were inoculated with 10^3 FFU of CHIKV-LR (n = 6, two experiments). At 8 hpi, 40 ng of 2,000-kDa FITC-dextran was injected into the ipsilateral footpad. Four hours later, DLNs were harvested and imaged using confocal microscopy. Scale bars, 200 μm. (H) The amount of FITC-dextran present was also determined after tissue homogenization by measuring the fluorescence signal (I) (n = 6, two experiments). Bars indicate median values. Statistical analysis: (D–G, and I) Mann-Whitney test; ns, not significant. See also Figure S1.

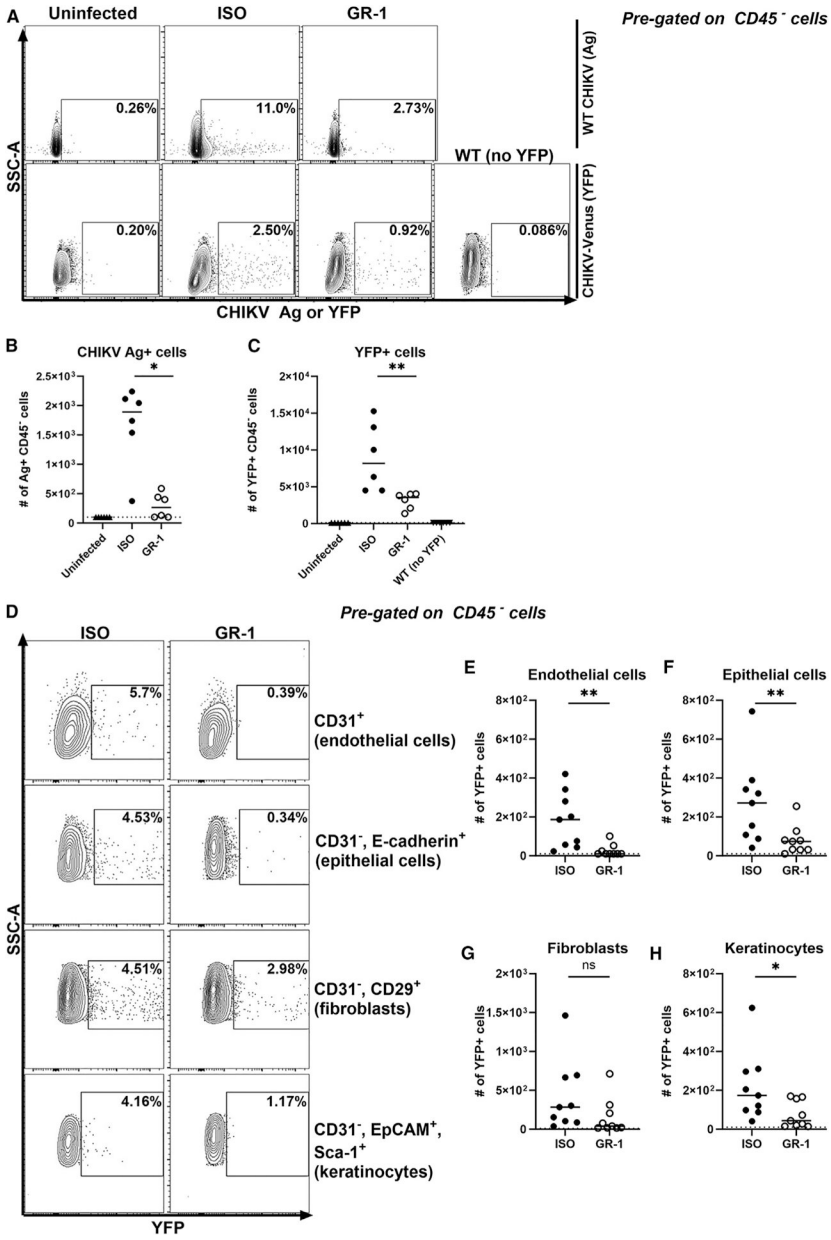

Figure 5. Ly6C/Ly6G cell depletion affects CHIKV replication in the CD45⁻non-hematopoietic cells in the skin

(A–C) Four-week-old male C57BL/6J mice were administered anti-GR-1 or isotype control antibody (day −1) and then inoculated in the footpad with 10^5 FFU of CHIKV AF15561-Venus reporter virus. Ipsilateral foot skin was harvested at 18 hpi and digested enzymatically to release stromal cells. Cell suspensions were incubated with anti-CD45 and anti-CHIKV E1, and flow cytometry was performed to assess the percentage (A) and number (B and C) of CD45⁻ cells expressing CHIKV antigen (Ag, A and B) or Venus (YFP, A and C) (n = 6, two experiments). Gating strategies are shown in Figure S4.

(D–H) Mice were administered anti-GR-1 or isotype control antibody and then inoculated with CHIKV-AF15561-Venus reporter virus. Ipsilateral foot skin was harvested at 18 hpi and digested enzymatically. Cell suspensions were incubated with anti-CD45, anti-CD31,

anti-E-cadherin, anti-EpCAM, anti-Sca-1, and anti-CD29 antibodies, and flow cytometry was performed to assess the percentage (D) and number of YFP^+ endothelial cells (E), epithelial cells (F), fibroblasts (G), and keratinocytes (H). (n = 9 or 10, two experiments) Naive controls were used to set staining gates for all samples. Bars indicate median values. Statistical analysis: (B, C, and E–H) Mann-Whitney test, *$p < 0.05$, **$p < 0.01$. See also Figures S1 and S5.

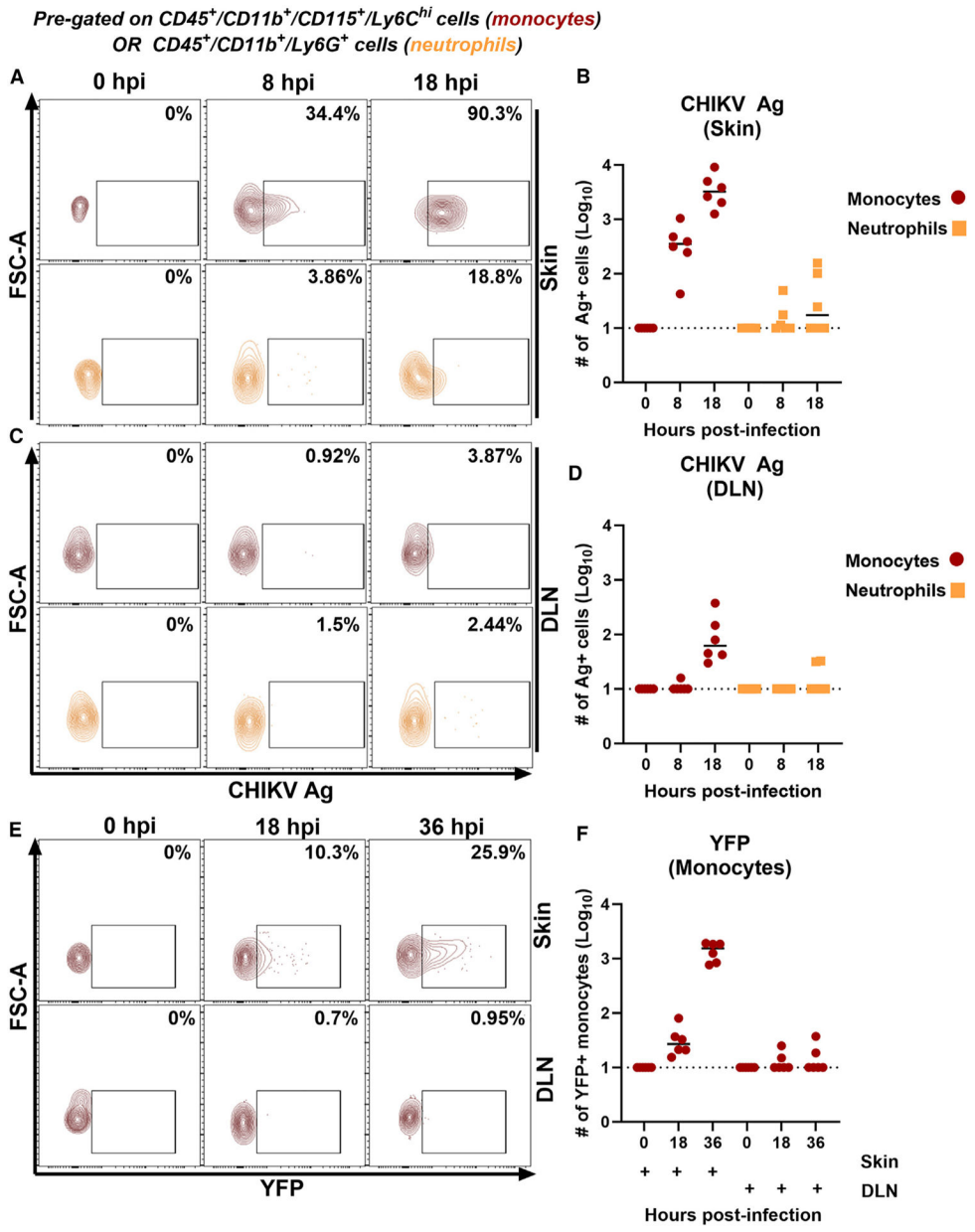

Figure 6. Monocytes in the skin support CHIKV infection

(A–D) Cohorts of 4-week-old male C57BL/6J mice were inoculated with 10^3 FFU of CHIKV-LR and sacrificed at 0, 8, or 18 hpi. Ipsilateral foot skin was harvested and processed. Cell suspensions were incubated with antibodies against CHIKV E1 (Ag), CD45, B220, CD3, NK1.1, Ly6G, Ly6C, CD115, and CD11b, and flow cytometry was performed to assess the percentages (A and C) and numbers (B and D) of $Ly6C^{hi}$ (monocytes, top panels) and $Ly6G^+$ (neutrophils, bottom panels) of cells expressing CHIKV antigen (n = 6, two experiments).

(E and F) Four-week-old C57BL/6J mice were inoculated in the footpad with 10^5 FFU of CHIKV AF15561-Venus reporter virus. At 0, 18, or 36 hpi, ipsilateral foot skin and DLN were harvested, and cell staining and flow cytometry were performed. The percentages (E)

and numbers (F) of Ly6C^{hi} monocytes expressing YFP are shown (n = 6, two experiments). Cells from naive mice were used to set staining gates. Gating strategies for this figure are shown in Figure S5. See also Figures S6 and S7. Bars indicate median values.

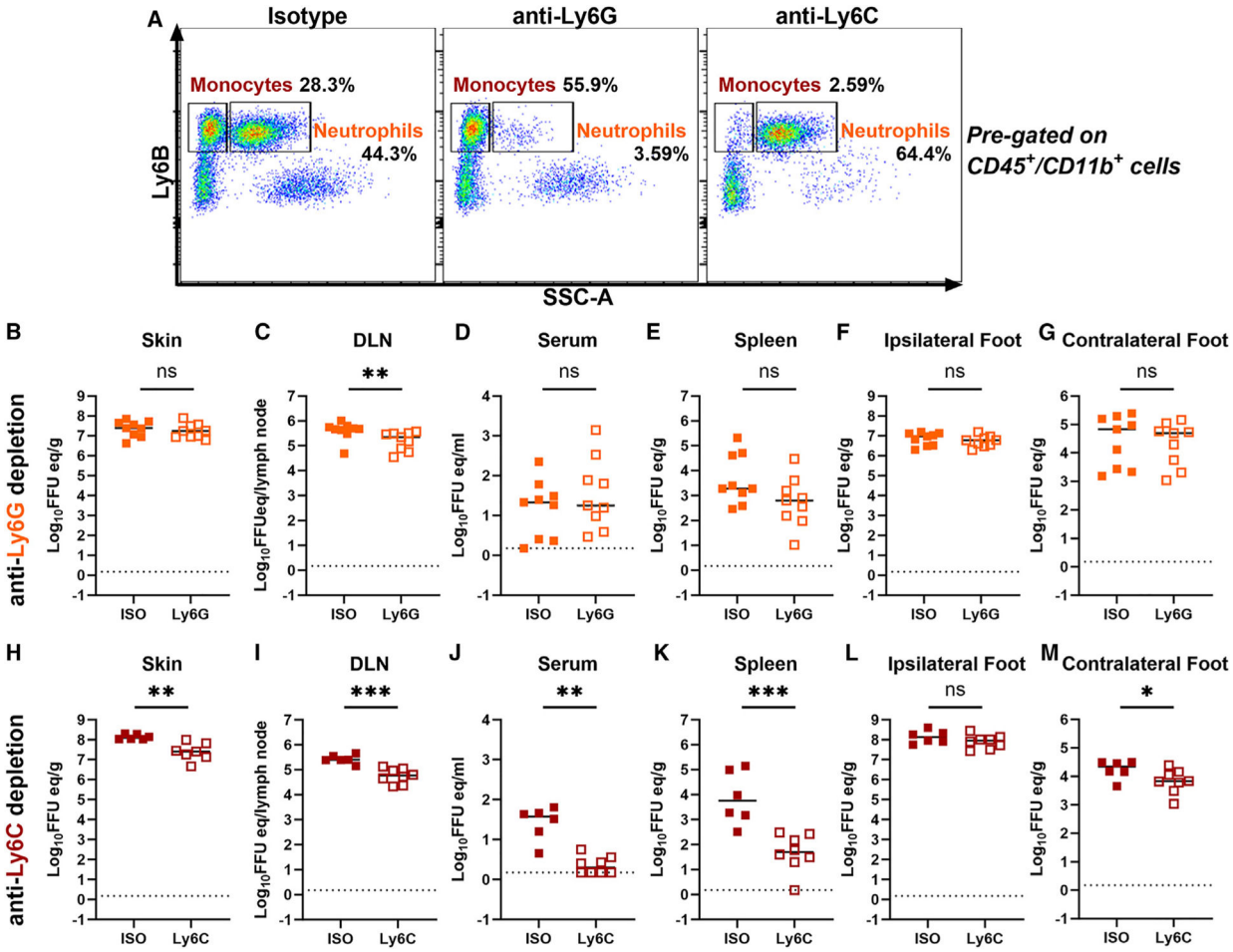

Figure 7. Depletion with anti-Ly6C but not anti-Ly6G antibodies reduces infection in the skin and delays CHIKV dissemination

(A) Representative flow plots showing monocyte and neutrophil depletions. Left, isotype control; middle, anti-Ly6G depletion; right, anti-Ly6C depletion. Populations are gated as follows: monocytes, $CD45^{+}B220^{-}CD3^{-}NK1.1^{-}CD11b^{+}Ly6B^{hi}$, side $scatter^{lo}$ cells; neutrophils, $CD45^{+}B220^{-}CD3^{-}NK1.1^{-}CD11b^{+}$, side $scatter^{hi}$ cells.

(B–M) Twenty-four hours prior to footpad inoculation with 10^{3} FFU of CHIKV-LR, cohorts of 4-week-old male C57BL/6J mice were administered anti-Ly6G (B–G), anti-Ly6C (H–M), or isotype control antibodies. At 18 hpi, ipsilateral foot skin (B and H), DLN (C and I), serum (D and J), spleen (E and K), ipsilateral feet (F and L), and contralateral feet (G and M) were harvested, and viral RNA was quantified by qRT-PCR (n = 6–9, two or three experiments). Bars indicate median values. Statistical analysis: Mann-Whitney test, ns, not significant, *$p < 0.05$, **$p < 0.01$, ***$p < 0.001$. See also Figure S1.

KEY RESOURCES TABLE

REAGENT or RESOURCE	SOURCE	IDENTIFIER
Antibodies		
Monoclonal rat anti-mouse Ly6C/Ly6G antibody clone RB6-8C5	BioXCell	Cat# BE0075 RRID:AB_10312146
Monoclonal rat anti-mouse Ly6C antibody clone Monts-1	BioXCell	Cat# BE0203 RRID:AB_2687696
Monoclonal rat anti-mouse Ly6G antibody clone 1A8	BioXCell	Cat# BP0075–1 RRID:AB_1107721
Monoclonal mouse anti-mouse IFNAR-1 antibody clone MAR1-5A3	Leinco Technologies	Cat# I-400 RRID:AB_2830666
Monoclonal human anti-alphavirus E1 antibody clone DC2.112	Kim et al., *Cell,* 2021[31]	N/A
Monoclonal mouse anti-alphavirus E1 antibody, clone CHK-166	Pal et al., *PLoS Pathogens,* 2014[55]	N/A
TruStain FcX monoclonal rat anti-mouse CD16/32	BioLegend	Cat#101320; RRID:AB_1574975
BUV395 anti-mouse CD45 clone 30-F11	BD Biosciences	Cat#564279; RRID:AB_2651134
BV421 anti-mouse B220 clone RA3-6B2	BioLegend	Cat#103251; RRID:AB_2562905
BV421 anti-mouse CD3 clone 145-2C11	BioLegend	Cat#100336; RRID:AB_10898314
PE/Cyanine7 anti-NK1.1 clone S17016D	BioLegend	Cat#156514; RRID:AB_2888852
PerCP/Cyanine5.5 anti-Ly6G clone 1A8	BioLegend	Cat#127616; RRID:AB_1877271
PE Dazzle anti-mouse/human CD11b clone M1/70	BioLegend	Cat#101256; RRID:AB_2563648
APC/Cyanine 7 anti-CD115 clone AFS98	BioLegend	Cat#135532; RRID:AB_2632740
FITC anti-mouse neutrophil antibody (Ly6B) clone 7/4	Abcam	Cat# ab53457; RRID:AB_881409
APC anti-mouse Ly6C clone HK 1.4	BioLegend	Cat#128016; RRID:AB_1732087
PE/Dazzle 594 anti-mouse CD31 clone 390	BioLegend	Cat#102430; RRID:AB_2566206
PE/Cyanine 7 anti-mouse/human E-cadherin clone DECMA-1	BioLegend	Cat#147310; RRID:AB_2564187
PE anti-mouse EpCAM clone G8.8	BioLegend	Cat#118206; RRID:AB_1134176
APC/Cyanine 7 anti-mouse Ly6A/E (Sca-1) clone D7	BioLegend	Cat#108126; RRID:AB_10645327
AF700 anti-mouse CD29 clone HMβ1-1	BioLegend	Cat#102218; RRID:AB_493711
Anti-mouse ER-TR7 clone ER-TR7	BioRad	Cat# MCA2402; RRID:AB_915429
FITC anti-mouse CD169 (Siglec-1) 3D6.112	BioLegend	Cat#142406 RRID:AB_2563106
Peroxidase-AffiniPure Goat Anti-Human IgG (H + L)	Jackson ImmunoResearch	Cat#109-035-003 RRID:AB_2337577
Bacterial and virus strains		
CHIKV LR-2006 OPY1	Fox et al., *Science Immunology,* 2019[56] Winkler et al., *Cell,* 2020[12] Fox et al., *PLoS Pathogens,* 2020[25]	N/A
CHIKV AF15561	Zhang et al., *Cell,* 2018[22] Zhang et al., *Cell Reports,* 2019[23]	N/A
RRV T48	Zhang et al., *Cell Reports,* 2019[23] Fox et al., *PLoS Pathogens,* 2020[25]	N/A
AURV	World Reference Center for Emerging Viruses and Arboviruses	N/A

REAGENT or RESOURCE	SOURCE	IDENTIFIER
	Toribio et al., *Journal of Virology,* 2020[28]	
Eilat-CHIKV 99659	Erasmus et al., *Nature Medicine,* 2017[29]	N/A
Critical commercial assays		
MagMAX-96 Viral RNA Isolation Kit	Applied Biosystems	Cat#AM1836
Taqman RNA-to-Ct 1-Step Kit	ThermoFisher	Cat#4392939
Experimental models: Cell lines		
Vero cells	ATCC	Cat#CCL-81; RRID:CVCL_0059
BHK-21[13] cells	ATCC	Cat#CCL-10; RRID:CVCL_1915
Aedes albopictus C6/36 cells	ATCC	Cat#CRL-1660 RRID:CVCL_Z230
Experimental models: Organisms/strains		
C57BL/6J mice	Jackson Laboratories	Strain#000664; RRID:IMSR_JAX:000664
MXRA8$^{\Delta 8/\Delta 8}$mice	Zhang et al., *Cell Reports,* 2019[23] (Ref. #23)	N/A
Oligonucleotides		
CHIKV-LR *E1* forward: 5′-TCGACGCGCCCTCTTCTTTAA-3′	IDT PrimeTime Assay	Custom (1 probe/2 primers)
CHIKV-LR *E1* reverse: 5′-ATCGAATGCACCGCACACT-3′	IDT PrimeTime Assay	Custom (1 probe/2 primers)
CHIKV-LR *E1* probe: 5′-/56-FAM/ACCAGCCTG/ZEN/ CACCCATTCCTCAGAC/3IABkFQ/-3′	IDT PrimeTime Assay	Custom (1 probe/2 primers)
CHIKV-LR *nsP1* forward: 5′-AAAGGGCAAACTCAGCTTCAC-3′	IDT PrimeTime Assay	Custom (1 probe/2 primers)
CHIKV-LR *nsP1* reverse: 5′-GCCTGGGCTCATCGTTATTC-3	IDT PrimeTime Assay	Custom (1 probe/2 primers)
CHIKV-LR *nsP1* probe: 5′-/56-FAM/CGCTGTGA/ZEN/ CAGTGGTTTCGTGTG/3IABkFQ/-3′	IDT PrimeTime Assay	Custom (1 probe/2 primers)
CHIKV-AF15561 *E1* forward: 5′-TCGACGCGCCATCTTTA-3′	IDT PrimeTime Assay	Custom (1 probe/2 primers)
CHIKV-AF15561 *E1* reverse: 5′-ATCGAATGCACCGCAC-3′	IDT PrimeTime Assay	Custom (1 probe/2 primers)
CHIKV-AF15561 *E1* probe: 5'-/56-FAM/ACCAGCC/ZEN/ TGCACCCACTCCTC/3IABkFQ/-3bgcolor = "#FFFFFF; " color = "#222222; ">′	IDT PrimeTime Assay	Custom (1 probe/2 primers)
AURV *E1* forward; 5′-CGGATCAAACCTGCACAATTC-3′	IDT PrimeTime Assay	Custom (1 probe/2 primers)
AURV *E1* reverse: 5′-TTCGTAGGTAAGGCAAGGTATTT-3′	IDT PrimeTime Assay	Custom (1 probe/2 primers)
AURV *E1* probe: 5bgcolor = "#FFFFFF; " color = "#222222; ">′-/56-FAM/ATACTCTG/ZEN/ CCACCAATGCATGGGA/3IABkFQ/-3bgcolor = "#FFFFFF; " color = "#222222; ">′	IDT PrimeTime Assay	Custom (1 probe/2 primers)
AURV *nsP3* forward 5′-CCACTGATATCCAACCCGAAG-3′	IDT PrimeTime Assay	Custom (1 probe/2 primers)
AURV *nsP3* reverse: 5′-GCCCATTTACTCAGACCTGTAG-3′	IDT PrimeTime Assay	Custom (1 probe/2 primers)
AURV *nsP3* probe: 5bgcolor = "#FFFFFF; " color = "#222222; ">′-/56-FAM/ACACCAAC/ZEN/ ACGATGCAGAACTATCTCC/3IABkFQ/-3bgcolor = "#FFFFFF; " color = "#222222; ">′	IDT PrimeTime Assay	Custom (1 probe/2 primers)
RRV *nsP3* forward: 5′-GTGTTCTCCGGAGGTAAAGATAG-3′	IDT PrimeTime Assay	Custom (1 probe/2 primers)
RRV *nsP3* reverse: 5′-TCGCGGCAATAGATGACTAC-3′	IDT PrimeTime Assay	Custom (1 probe/2 primers)
RRV *nsP3* probe: 5bgcolor = "#FFFFFF; " color = "#222222; ">′-/56-FAM/ACCTGTTTA/ZEN/ CCGCAATGGACACCA/3IABkFQ/-3bgcolor = "#FFFFFF; " color = "#222222; ">′	IDT PrimeTime Assay	Custom (1 probe/2 primers)

REAGENT or RESOURCE	SOURCE	IDENTIFIER
EILV-CHIKV *E1* forward: 5′-TGGAGCTTCTGTCTGTCACC-3′	IDT PrimeTime Assay	Custom (1 probe/2 primers)
EILV-CHIKV *E1* reverse: 5′-ACGTACGGAGACGGGATAAC-3′	IDT PrimeTime Assay	Custom (1 probe/2 primers)
EILV-CHIKV E1 probe: 5bgcolor = “#FFFFFF; ” color = “#222222; ”>′-/56-FAMTCGCTTGAT/ZEN/TACATC/ACG/TGC/CAG/3IABkFQ/-3bgcolor = “#FFFFFF; ” color = “#222222; ”>′	IDT PrimeTime Assay	Custom (1 probe/2 primers)
Mus musculus Gapdh primer + probe	IDT PrimeTime Assay	Mm.PT.39a.1
Software and algorithms		
FlowJo	BD Biosciences	V10.8.1; RRID:SCR_008520
GraphPad Prism	GraphPad	V10.1.2; RRID:SCR_002798
FIJI	ImageJ2	V2.9.0/1.53t; RRID:SCR_002285
Imaris	Oxford Instruments	V8.0; RRID:SCR_007370
Zen	Zeiss Microscopy	RRID:SCR_013672
BioRender	BioRender	RRID:SCR_018361
Other		
Gibco 0.05% trypsin-EDTA	Thermo Fisher	Cat#25300054
DNase I	Sigma Aldrich	Cat#D4263
Liberase TL	Millipore Sigma (Roche)	Cat# 05401020001
Dispase II	Millipore Sigma (Roche)	Cat# 04942078001